View metadata, citation and similar papers at core.ac.uk

brought to you by CORE

provided by Clemson University: TigerPrints

Clemson University
TigerPrints

All Theses | Theses

12-2013

Adaptive Transmission for OFDM

Michael Juang
Clemson University, michael.juang@gmail.com

Follow this and additional works at: https://tigerprints.clemson.edu/all_theses


Part of the Electrical and Computer Engineering Commons

Recommended Citation
Juang, Michael, "Adaptive Transmission for OFDM" (2013). *All Theses*. 1795.
https://tigerprints.clemson.edu/all_theses/1795

This Thesis is brought to you for free and open access by the Theses at TigerPrints. It has been accepted for inclusion in All Theses by an authorized administrator of TigerPrints. For more information, please contact kokeefe@clemson.edu.

ADAPTIVE TRANSMISSION FOR OFDM

A Thesis
Presented to
the Graduate School of
Clemson University

In Partial Fulfillment
of the Requirements for the Degree
Master of Science
Electrical Engineering

---

by
Michael A. Juang
December 2013

Accepted by:
Dr. Michael B. Pursley, Committee Chair
Dr. Daniel L. Noneaker
Dr. Harlan B. Russell

Abstract

To respond to dynamic channel conditions caused by fading, shadowing, and other time-varying disturbances, orthogonal frequency division multiplexing (OFDM) packet radio systems should adapt transmission parameters on a packet-by-packet basis to maintain or improve performance over the channel. For this to be possible, there are three key ideas that must be addressed: first, how to determine the subchannel conditions; second, which transmission parameters should be adapted; and third, how to adapt those parameters intelligently. In this thesis, we propose a procedure for determining relative subchannel quality without using any traditional channel measurements. Instead, statistics derived solely from subcarrier error counts allow subchannels to be ranked by order of estimated quality; this order can be exploited for adapting transmission parameters. We investigate adaptive subcarrier power allocation, adaptive subcarrier modulation that allows different subcarriers in the same packet to use different modulation formats, and adaptive coding techniques for OFDM in fading channels. Analysis and systems simulation assess the accuracy of the subcarrier ordering as well as the throughput achieved by the proposed adaptive transmission protocol, showing good performance across a wide range of channel conditions.

Table of Contents

List of Tables

List of Figures

Chapter 1

Introduction

OFDM has become a part of many wireless communications systems, and it has gained adoption in many communications protocols and standards for both wireless local area networks and broadband wireless access. OFDM is a multi-carrier modulation technique that is effective in combating frequency-selective fading in broadband wireless channels. The main characteristic of interest is that it subdivides the available frequency band into multiple subchannels, transmitting simultaneously on each. OFDM waveform generation and the details of transmission and reception are described in [1–3].

For frequency-selective channels, channel conditions may be significantly vary from one subchannel to another. Furthermore, the severity of the fading may change over time, and the channel could experience dynamic shadowing and interference as well. As a result many adaptive transmission schemes have been proposed in the literature suggesting methods to change parameters such as transmission power, modulation formats, and coding in response to the dynamics of the channel. Sometimes the power adaptation is called *power loading*, while likewise the adaptive modulation is known as *bit loading* because the number of bits per modulation symbol is governed by which modulation format is chosen. Primarily the focus has been on power loading, bit loading, or both, with the effects of

error-control often not considered.

Much of the prior research on power loading [4–6] and/or bit loading [7–10] assumes that the transmitter has perfect channel state information (CSI), so it knows the exact fade level for each subcarrier. This level of information would require extensive, perfectly accurate channel measurements to assess previous conditions and then perfect future prediction to guess the upcoming state of the channel; thus, it is not realistic for practical communications. However, even the research that considers imperfect channel state information either supposes noisy channel state estimation [11, 12] or limited or quantized feedback information [13, 14]. There is still the assumption that the receiver has the hardware and ability, in the idealized channel conditions considered, to make fairly good estimates of the channel conditions.

In this thesis we consider the suitability for power loading for wireless OFDM communications with the assumption that error-control coding is used. Then attention is turned to focus on a practical alternative to channel gain estimation for ordering subcarriers by estimated channel quality. Rather than directly measure the channel, statistics from the decoder are used to determine relative subchannel conditions and rank them in by estimated order of quality. This ordering information can then be used to assign modulation formats and code rates for each subcarrier on a packet-by-packet basis. We describe an entire adaptive modulation and coding protocol based on these statistics. Previously, ranking or ordering subcarriers as part of the basis for power loading was considered in [14] and for bit loading in [10, 15], but the mechanism for determining the subchannel ranking is much different here. The new ranking-based approach is developed and evaluated, and we make different assumptions about the channel and describe the adaptive modulation and coding with greater detail.

Chapter 2

System Description

OFDM packet radio systems may be able to adapt the subcarrier power levels, modulation formats, and error-control coding on a packet-to-packet basis in response to changing channel conditions. In particular, we examine half-duplex communications, so feedback information for adaptation must be relayed back to the transmitter, which could be accomplished in acknowledgment packets. In Section 2.1 the channel fading model is described, while details about the packet transmission parameters are given in 2.2.

2.1 Channel fading model

Assessing adaptive transmission protocols for OFDM packet radio communications requires a suitable model and assumptions about the dynamically-varying channel conditions. The focus is on the effects of frequency-selective fading and how this variation across time and across different subcarriers motivate the use of adaptive modulation and coding protocols. As such, the usual assumptions in the literature are taken; we assume perfect sampling, pulse shaping, and synchronization. For an OFDM system with $\mathcal{N}$ subcarriers, the subcarriers are indexed by $i \in \{1,\ldots,\mathcal{N}\}$. At the receiver, the gain for subchannel i corresponding to the fading on the subchannel i is H_i, and the channel-gain vector is $\boldsymbol{H} = [H_1\ H_2\ \ldots\ H_{\mathcal{N}}]$. Thus, the average received energy for a modulation symbol on

subcarrier i is $|H_i|^2\mathscr{E}_m$, where $\mathscr{E}_m$ denotes the average transmitted energy per modulation symbol.

Taking N_0 to be the one-sided power spectral density for the thermal noise, the received energy to noise-density ratio for subcarrier i is $\xi_i = |H_i|^2\mathscr{E}_m/N_0$ in the absence of adjustments by power loading. The received modulation symbol energy to noise-density ratio (MENR) in decibels for a subcarrier i is $\text{MENR}_i = 10\log_{10}(\xi_i)$. As a reference point, we denote the received energy to noise-density ratio in the absence of fading as ξ^*. The subscript is dropped because all subcarriers would have the same ratio without fading, so ξ^* is the common reference point. Similarly, the modulation symbol energy to noise-density ratio in the absence of fading is $\text{MENR}^* = 10\log_{10}(\xi^*)$. Thus, MENR^* can be considered the nominal signal-to-noise ratio.

For some of the empirical evaluations and analysis, we use N-state Markov chains to model the time variation of the fading channels. In particular, we consider Nakagami-m fading [16, 17] for different values of the parameter m including the special case of $m = 1$, which is Rayleigh fading. Each state of the Markov chain corresponds to a different fade level. We assume that the channel conditions remain static throughout each transmission, which is reasonable if the fading is not very fast. Between each packet transmission, the Markov chain state representing the channel may change, with probabilities given by the model's state transition probabilities. For all the results presented in this thesis, there are $N = 12$ states in the Markov chain. This allows suitable granularity in representing fade levels while limiting the number of states to a level reasonable for analysis.

The state transition probabilities for the Markov chains and the fade level corresponding to each Markov chain state are determined from the parameters of the Nakagami-m fading. The two parameters are m and the normalized Doppler frequency f_dT_s, which is the product of the Doppler frequency f_d and the time T_s between one packet and the next. For convenience we assume f_dT_s is constant for a communications session. If a commu-

nications protocol is successful over a wide range of values for $f_d T_s$, it should be suitable for channel conditions in which the Doppler or time between packets may vary. The methods in which Markov chain parameters can be selected to match specific fading models is described in more detail in [18].

In addition, the fading channels encountered by an OFDM communications system may be significantly correlated in frequency so some adjacent subcarriers have similar conditions. For our performance results, we consider a hypothetical worst-case fading scenario in which the fading for different subcarriers is modeled by $\mathcal{N}$ independent (and identical) Markov chains; in the other extreme, the fading is the same for all subcarriers and it is modeled by a single Markov chain. However, our focus is primarily on a case between the extremes, in which some subcarriers are modeled by one Markov chain, other subcarriers by another independent one, and so on, with one independent Markov chain for each of $\mathcal{G}$ groupings of subcarriers. This model may be especially appropriate when considering OFDM-based systems in which subcarriers are spread among multiple non-contiguous frequency bands.

2.2 System model and evaluation

For performance evaluations of hypothetical ideal protocols and practical adaptive modulation and coding protocols in this thesis, we consider OFDM with bit-interleaved coded modulation [19]. There are $\mathcal{N} = 64$ subcarriers for the numerical evaluations of OFDM, but the procedures and conclusions drawn in this thesis are applicable to a wider range of OFDM systems and numbers of subcarriers. Each subcarrier uses Gray-coded QPSK, 16-QAM, or 64-QAM modulation; different subcarriers may use different modulation formats for adaptive modulation, but within a packet each individual subcarrier does not switch between modulation formats. The symbols transmitted on the individual subcar-

riers are referred to as *modulation symbols*, and the receiver employs optimum coherent demodulation. It is assumed that the orthogonality of all subcarriers is perfectly maintained. All modulation symbols for each subcarrier have the same duration, so the bandwidth is the same for each subcarrier and packet transmission. Likewise, the QPSK and 16-QAM constellations are normalized to maintain the same average energy per modulation symbol.

For the error-control coding, the interleaved data is encoded with one of five block codes from a family of turbo product codes [20] with rates approximately 0.236, 0.325, 0.495, 0.660, and 0.793. The block lengths of the five codes divide evenly into 4096. The receiver uses iterative soft-decision decoding. Only if all code blocks within a packet can be decoded successfully do we consider the transmission to be a success. As is usual, a cyclic redundancy check code can be used to determine if the packet is successful or not. Because code symbols are transmitted on different subcarriers, each with potentially different channel conditions, the performance of the iterative decoding cannot be readily calculated or predicted. There is a high interdependence between decoding performance and all the transmission parameters selected, as well as all of the current subchannel conditions. The turbo product codes are used for illustrative purposes and consistency with prior research; any other high-performance code with iterative decoding, including LDPC codes, would also be appropriate.

For each packet, L binary code symbols are transmitted, where L is always chosen to be 4096 or another multiple of 4096 such as 8192 and 16384. For a packet of length L, the number of information bits in each packet thus depends on the code rate, and the duration of each packet depends on the modulation formats used by each subcarrier. An OFDM block $\mathcal{B}$ is defined to be the collection of all $\mathcal{N}$ modulation symbols, one per subcarrier, being transmitted at any given time. As a result, the number of OFDM blocks per packet and thus the packet durations depend on L as well as the individual subcarrier modulations used.

Chapter 3

Power loading

Adaptive power allocation on subcarriers can be applied to OFDM transmissions as subchannel conditions vary over time. Power loading has been suggested as a solution for dynamic fading on multicarrier modulation systems though less frequently for wireless OFDM systems. Even more so than adaptive modulation or coding, adaptive subcarrier power loading requires accurate information about the subcarrier channel conditions, which is more challenging if the fading or other channel perturbances are more dynamic.

Section 3.1 provides background information on the modulation formats considered, bit error rates, and bit error rate approximations, which are used for the development of the power loading algorithms in Section 3.2. Then, the benefits and drawbacks of power loading are explored and discussed in Section 3.3.

3.1 Subcarrier modulation

We consider power loading subject to a constraint on the total power in the transmitted OFDM signal, but there is no restriction on how the total power is allocated among the $\mathcal{N}$ subcarriers. OFDM has a high peak-to-average power ratio and relies on linearity of the amplifier to maintain orthogonality between subcarriers; therefore, it is especially important to constrain the total power in the OFDM signal. Also, increases in transmitted

power can make the signal easier to detect by unauthorized receivers and also increases the interference to other systems operating in the same frequency band. Based on these considerations, the total transmitted power is kept constant.

For subcarrier $i \in \{1,\ldots,\mathcal{N}\}$, the power loading coefficient is defined by $\mu_i = \mathcal{N}P_T^{(i)}/P_T$, where P_T represents the total power and $P_T^{(i)}$ is the subcarrier power. Therefore, the power constraint is

$$\sum_{i=1}^{\mathcal{N}} \mu_i = \mathcal{N} = \text{constant}. \tag{3.1}$$

The power-loading vector for the OFDM signal is $\boldsymbol{\mu} = [\mu_1\ \mu_2\ \ldots\ \mu_{\mathcal{N}}]$. We let $\mathscr{E}_m$ denote the average energy per modulation symbol in the transmitted signal. As given in the previous chapter, the subchannel gain on subcarrier i is H_i, and the channel-gain vector is $\boldsymbol{H} = [H_1\ H_2\ \ldots\ H_{\mathcal{N}}]$. If there is no power loading, then $\mu_i = 1$ and the received energy for the modulation symbol on subcarrier i is $|H_i|^2\mathscr{E}_m$. We define $\gamma_i = |H_i|^2\mathscr{E}_m/N_0$, where N_0 is the one-sided power spectral density for the thermal noise. The received energy to noise-density ratio for subcarrier i is then $\xi_i = \gamma_i\mu_i$.

The following expressions for $P_{e,i}^{(M)}$, the average probability of binary symbol error on subchannel i, are given in terms of the Gaussian Q function, which is the complementary distribution function for a zero-mean, unit-variance Gaussian random variable. For each M, Gray coding is employed in the assignment of binary symbols to M-QAM symbols, and the average is computed over all modulation symbols in the QAM constellation and over all bit positions for each modulation symbol. For 4-QAM, the exact expression is

$$P_{e,i}^{(4)} = Q\left(\sqrt{\xi_i}\right). \tag{3.2}$$

For 16-QAM, the exact error probability is given by

$$P_{e,i}^{(16)} = \frac{3}{4}Q\left(\sqrt{\frac{1}{5}\xi_i}\right) + \frac{1}{2}Q\left(\sqrt{\frac{9}{5}\xi_i}\right) - \frac{1}{4}Q\left(\sqrt{5\xi_i}\right), \tag{3.3}$$

and the exact expression for 64-QAM is

$$\begin{aligned} P_{e,i}^{(64)} = {} & \frac{7}{12}Q\left(\sqrt{\frac{1}{21}\xi_i}\right) + \frac{1}{2}Q\left(\sqrt{\frac{3}{7}\xi_i}\right) - \frac{1}{12}Q\left(\sqrt{\frac{25}{21}\xi_i}\right) \\ & + \frac{1}{12}Q\left(\sqrt{\frac{27}{7}\xi_i}\right) - \frac{1}{12}Q\left(\sqrt{\frac{169}{21}\xi_i}\right). \end{aligned} \tag{3.4}$$

Previous investigations of power loading, including [4], have used various approximations of the form

$$P_{e,i}^{(M)} \approx \frac{L_M}{\log_2(M)}\, Q\left(\sqrt{3\xi_i/(M-1)}\right). \tag{3.5}$$

For example, a union bound can be applied to the symbol error probability [21] and then the symbol error probability can be divided by $\log_2(M)$. This leads to $L_M = 4$ (as in [21] and [22]). When the SNR ξ_i is high, the expression on the right of (3.5) is a good approximation to the upper bound on $P_{e,i}^{(M)}$. Another approximation for the error probabilities is obtained by using only the first term of the exact expression for $P_{e,i}^{(M)}$, which is a lower bound that improves with higher ξ_i. The values of L_M for the first terms in (3.2)–(3.4) are $L_4 = 2$, $L_{16} = 3$, and $L_{64} = 3.5$. As $M \to \infty$, a greater percentage of the points in the M-QAM constellation are on the interior, and $L_M \to 4$.

The problem with these various approximations is that they are inaccurate for ranges of ξ_i practically encountered by in OFDM systems with modern error-control coding. Though the approximations may be suitable for high signal-to-noise ratios, systems with good error-control codes do not require a high signal-to-noise ratio. The inaccuracies of the two approximations are demonstrated across a range of SNR for 16-QAM in Fig. 3.1

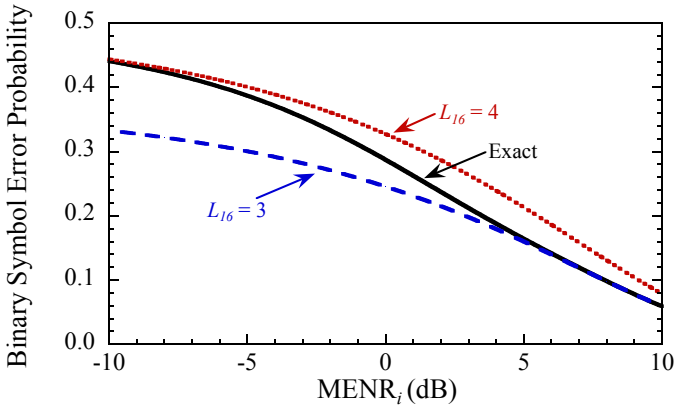

Figure 3.1: Exact and approximate error probabilities for 16-QAM.

for $M = 16$. The union-bound approximation is labeled with $L_{16} = 4$ and overestimates the probability of error; the curve labeled with $L_{16} = 3$ is the first-term approximation, which is better at higher SNR. A sudden fade in the channel, shadowing, or simply a small power loading coefficient could all cause subchannel i to have low MENR$_i$. In these cases, MENR$_i$ could easily drop below 0 dB, whereupon both approximations are not good. Thus, we make use of the exact bit error probability expressions in the next section and do not rely on the approximations.

3.2 Power loading algorithms for OFDM

The goal for power loading should be to improve the system performance over the channel as $\boldsymbol{H}$ changes over time. Because of the channel coding, the power allocation that achieves the greatest packet success rate is difficult or impossible to determine even if $\boldsymbol{H}$ is completely known. Nevertheless, the power allocation that achieves the lowest code symbol error rate over the channel prior to decoding can be calculated. We call this the *minimum BER power loading*, where BER stands for the hard-decision bit (binary symbol) error rate prior to decoding. This min BER power loading makes no guarantee about the

packet error rate for a system with error-control coding and soft-decision decoding.

We determine the minimum BER power loading through the Lagrange method for every transmission, following the overall approach in [4] but generalizing it so different modulation formats are allowed for different subcarriers. Furthermore, we use the exact probability of hard-decision error at the demodulator rather than one of the approximations given in Section 3.1. Were the approximations used instead, the minimum BER power loading algorithm would not truly minimize the BER. The goal is to minimize the average probability of error $f(\boldsymbol{\mu})$ subject to the power constraint $g(\boldsymbol{\mu}) = \mathcal{N}$. The Lagrange function is

$$\Lambda(\boldsymbol{\mu}, \lambda) = f(\boldsymbol{\mu}) + \lambda [g(\boldsymbol{\mu}) - \mathcal{N}]. \tag{3.6}$$

The modulation formats used in each subcarrier are considered as statically allocated and constant while solving for $\boldsymbol{\mu}$. Let N_i represent the number of code symbols transmitted in a packet on subcarrier i and $N = \sum_{i=1}^{\mathcal{N}} N_i$ be the total number of code symbols in the packet. Then

$$f(\boldsymbol{\mu}) = \frac{1}{N} \sum_{i=1}^{\mathcal{N}} N_i P_{e,i}, \tag{3.7}$$

$$g(\boldsymbol{\mu}) = \sum_{i=1}^{\mathcal{N}} \mu_i = \mathcal{N}. \tag{3.8}$$

The solution to the minimization problem is given by solving

$$\nabla \Lambda(\boldsymbol{\mu}, \lambda) = \nabla (f(\boldsymbol{\mu}) + \lambda [g(\boldsymbol{\mu}) - \mathcal{N}]) = 0. \tag{3.9}$$

The expression in (3.9) is equivalent to the following system of equations, for $i = 1, \ldots, \mathcal{N}$:

$$\begin{aligned}\frac{\partial \Lambda(\boldsymbol{\mu}, \lambda)}{\partial \mu_i} &= \frac{N_i}{N} \frac{\partial}{\partial \mu_i}(P_{e,i}) + \frac{\partial}{\partial \mu_i}\left[\lambda\left(\sum_{i=1}^{N}(\mu_i) - N\right)\right] \\ &= \frac{N_i}{N} \frac{\partial}{\partial \mu_i}(P_{e,i}) + \lambda \;=\; 0, \qquad (3.10)\\ \frac{\partial \Lambda(\boldsymbol{\mu}, \lambda)}{\partial \lambda} &= \sum_{i=1}^{N}(\mu_i) - N \;=\; 0. \qquad (3.11)\end{aligned}$$

If all $\mathcal{N}$ subcarriers use the same modulation format, then $N_i/N_{tot} = 1/\mathcal{N}$. The partial derivative with respect to μ_i is

$$\begin{aligned}\frac{\partial}{\partial \mu_i} P_{e,i}^{(4)} &= -\left\{\exp\left(-\frac{\gamma_i \mu_i}{2}\right)\right\}\left\{\sqrt{\frac{\gamma_i}{8\pi\mu_i}}\right\}, \qquad (3.12)\\ \frac{\partial}{\partial \mu_i} P_{e,i}^{(16)} &= -\left\{\frac{3}{4}\exp\left(-\frac{\gamma_i \mu_i}{10}\right) + \frac{3}{2}\exp\left(-\frac{9\gamma_i \mu_i}{10}\right) - \frac{5}{4}\exp\left(-\frac{25\gamma_i \mu_i}{10}\right)\right\} \\ &\quad \left\{\sqrt{\frac{\gamma_i}{40\pi\mu_i}}\right\}, \qquad (3.13)\\ \frac{\partial}{\partial \mu_i} P_{e,i}^{(64)} &= -\left\{\frac{7}{12}\exp\left(-\frac{\gamma_i \mu_i}{42}\right) + \frac{3}{2}\exp\left(-\frac{9\gamma_i \mu_i}{42}\right) - \frac{5}{12}\exp\left(-\frac{25\gamma_i \mu_i}{42}\right)\right. \\ &\quad \left. + \frac{3}{4}\exp\left(-\frac{81\gamma_i \mu_i}{42}\right) - \frac{13}{12}\exp\left(-\frac{169\gamma_i \mu_i}{42}\right)\right\}\left\{\sqrt{\frac{\gamma_i}{168\pi\mu_i}}\right\}, \qquad (3.14)\end{aligned}$$

for $M = 4, 16$, and 64. Recall that $\xi_i = \gamma_i \mu_i$ was used for convenience in the prior section. Thus, the power loading allocation vector $\boldsymbol{\mu}$ is the solution to a system of $\mathcal{N}$ transcendental equations with the total power constraint equation. Solving the system of equations requires numerical methods that would be infeasible for a tactical communications system to implement on a packet-by-packet basis.

Another power loading strategy is to transmit with more power on subcarriers that experience deeper fading and less power on those with good subchannel conditions in order to make the received SNR equal on each subcarrier. We call this the *equalizing power*

loading. Again, this loading requires the transmitter to know the precise subchannel fading. The power loading coefficients are calculated by

$$\mu_i = \frac{\mathcal{N}|H_i|^{-2}}{\sum_{j=1}^{\mathcal{N}} |H_j|^{-2}}, \quad 1 \leq i \leq \mathcal{N}. \tag{3.15}$$

Also proposed in [4] is a *quasi-optimal power loading* that is computationally much simpler than the minimum BER power loading. Like the other power loading algorithms, it requires accurate channel state information. Quasi-optimal power loading approximates minimum BER loading in the sense that at low SNR more power is allocated to the best subcarriers, and at high SNR more power is allocated to the worst subcarriers. The power loading coefficients for this algorithm are

$$\mu_i = \mathcal{N}\frac{b_i}{1+b_i^2}\left(\sum_{j=1}^{\mathcal{N}} \frac{b_j}{1+b_j^2}\right)^{-1}, \quad 1 \leq i \leq \mathcal{N}, \tag{3.16}$$

with $b_i = |H_i|^2 K_M \gamma_i$. H_i, K_M, and γ_i are defined as in Section 3.1.

Finally, the system may not use any power loading at all, just allocating the same amount of power to each subcarrier. We call this *no power loading*, or *no PL*, which has the advantage of lowest complexity and does not require any channel state information. In most systems, as in the remainder of this thesis, if power loading is not mentioned, it can be assumed that there is no power loading. The power loading coefficients are given by

$$\mu_i = 1, \quad 1 \leq i \leq \mathcal{N}. \tag{3.17}$$

3.3 Power loading evaluation

In this section the power loading algorithms described in Section 3.2 are evaluated for slow frequency-selective fading channels. The power loading algorithms are applied to OFDM systems using the same modulation format on each subcarrier (i.e. without bit loading), though this restriction is not a requirement for any of the power loading algorithms considered. Unlike in many other investigations of power loading, we incorporate the effects and benefits of error-control coding.

As an introductory example, the power loading algorithms are demonstrated in Figs. 3.2 and 3.3 for a slow Rayleigh fading channel for an OFDM system that has $\mathcal{N} = 16$ subcarriers and uses 16-QAM with the rate 0.236 code. The power loading coefficients μ_i generated by each power loading algorithm are given in Table 3.1. The curves in Fig. 3.2 show the received MENR that result from the power loading algorithms being applied to the same fading channel. Note that the no PL case shows the received MENR across the range of subcarriers (frequency) when equal power is transmitted on every subcarrier, so it is proportional to the channel gain over the frequency band of the OFDM signal. In this example, subcarrier 7 suffers the deepest fading, which causes the quasi-optimal and minimum BER algorithms to allocate power away from it.

The uncoded bit error rate that results from the power loading is shown in Fig. 3.3. Equalizing loading clearly has the worst performance. No power loading, quasi-optimal loading, and minimum BER loading all perform about the same in terms of the hard decision uncoded bit error rate. This is typical for low values of MENR. The uncoded bit error rate averaged over all the subcarriers is given in Table 3.2, along with the resulting packet error rate and throughput.

The quasi-optimal power loading achieves the lowest packet error rate (PER) and thus the best throughput, even though it incurs slightly larger uncoded BER than other

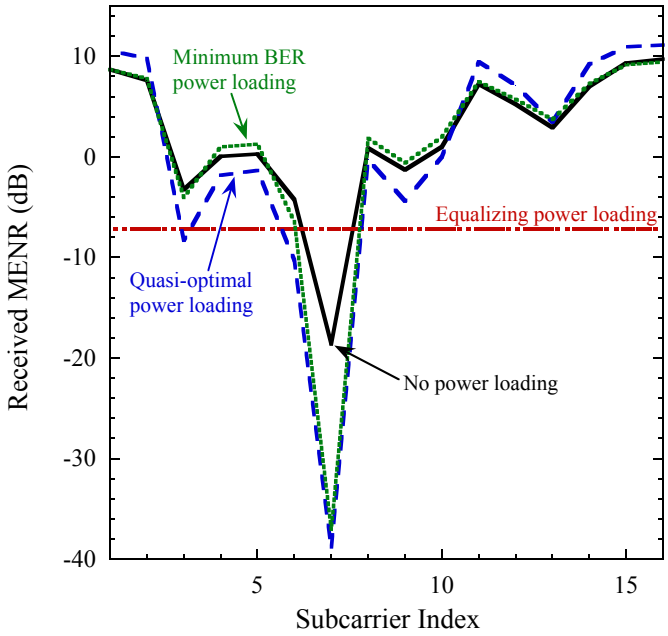

Figure 3.2: Received MENR for different power loading algorithms subjected to the same channel conditions.

forms of power loading. Because of the soft-decision decoding, information from the worst subcarriers is weighted less heavily; therefore, allocating power away from poor subcarriers is particularly beneficial in low MENR conditions. Again we note that minimizing the uncoded BER does not minimize the PER. Furthermore, the set of coefficients $\boldsymbol{\mu}$ that actually minimizes the PER cannot be calculated readily because of the complexity of the soft-decision iterative decoding.

To simulate the time-varying subchannel fade levels, finite-state Markov chains are used, with one Markov chain corresponding to each subchannel. The state transition probabilities and fade levels for each Markov chain state are set to approximate a Rayleigh fading channel according to common methods [23].

The uncoded bit error rate is given in Fig. 3.4 for QPSK, 16-QAM, and 64-QAM without power loading, with quasi-optimal power loading, and with minimum BER power

Subcarrier	No PL	Equalizing	Quasi-opt	Min BER
1	1.000	0.0258	1.5466	0.9962
2	1.000	0.0330	1.6507	1.0418
3	1.000	0.4038	0.3132	0.8372
4	1.000	0.1887	0.6498	1.2454
5	1.000	0.1782	0.6845	1.2499
6	1.000	0.5085	0.2496	0.6063
7	1.000	13.8275	0.0092	0.0143
8	1.000	0.1562	0.7706	1.2520
9	1.000	0.2559	0.4878	1.1698
10	1.000	0.1514	0.7922	1.2510
11	1.000	0.0360	1.6653	1.0547
12	1.000	0.0570	1.5439	1.1167
13	1.000	0.0974	1.1351	1.2010
14	1.000	0.0380	1.6684	1.0623
15	1.000	0.0223	1.4509	0.9625
16	1.000	0.0203	1.3822	0.9389

Table 3.1: Power loading coefficients μ_i for Figs. 3.2 and 3.3.

	No PL	Equalizing	Quasi-opt	Min BER
BER, theoretical	0.222018	0.415189	0.226618	0.216667
BER, simulated	0.222019	0.415188	0.226619	0.216662
Coded PER	0.102109	1.000000	0.019741	0.019984
Throughput	1738.32	0.00	1897.78	1897.31

Table 3.2: Summary of results for Figs. 3.2 and 3.3.

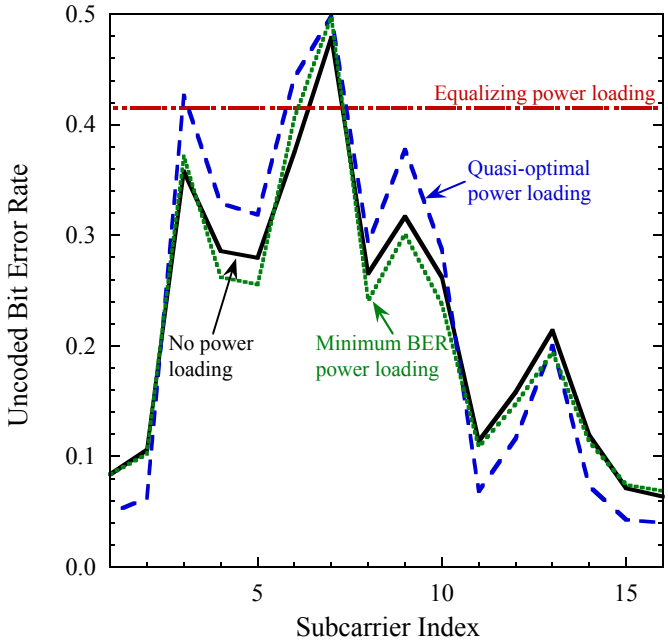

Figure 3.3: Uncoded bit error rate for different power loading algorithms with 16-QAM modulation for the channel in Fig. 3.2.

loading. The corresponding packet error rate for the rate 0.495 code is shown in Fig. 3.5. Equalizing power loading has poor performance and is omitted for legibility. Each data point represents the BER or PER for a separate simulation in which the subchannels are allowed to evolve over 5 million packets, and the MENR for the data point is given as the average over all subcarriers over time. The minimum BER power loading has approximately the same packet error rate as the quasi-optimal power loading over much of the range of MENR. To achieve a packet error rate of 0.01, a system without power loading requires 0.5 dB greater MENR for QPSK, 0.4 dB greater for 16-QAM, and 1.5 dB greater for 64-QAM relative to a system using minimum BER power loading. Although power loading can make a large difference in the uncoded hard decision bit error rate at high MENR, the difference in PER is not large in the range of MENR of interest.

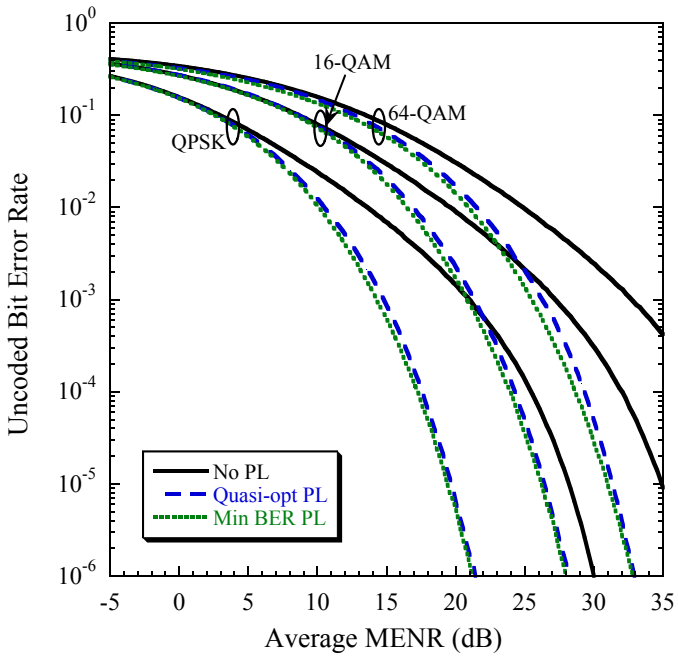

Figure 3.4: Binary hard-decision error rate for different power loading algorithms and modulation formats, using the rate 0.495 code, $\mathcal{N} = 16$ subcarriers.

3.4 Power loading compared to adaptive modulation and coding

It has been noted that "accurate receiver channel state information (CSI) is required at the transmitter" to "achieve the performance advantages of adaptive modulation" [11]. Despite this, an adaptive modulation and coding protocol for OFDM that does not rely on traditional CSI is described later in Chapter 5. However, for the moment we are only interested in evaluating the merits of power loading against those alternatives.

Now we look at the average throughput per transmission of 16-QAM with the rate 0.495 code using minimum BER power loading in Fig. 3.6 and compare its performance to different adaptive modulation and coding schemes. The method by which modulation formats and error-control codes can be selected, as well as a description of the hypothetical Perfect State Information for the Next packet (PSI-N) benchmark protocol, will be detailed

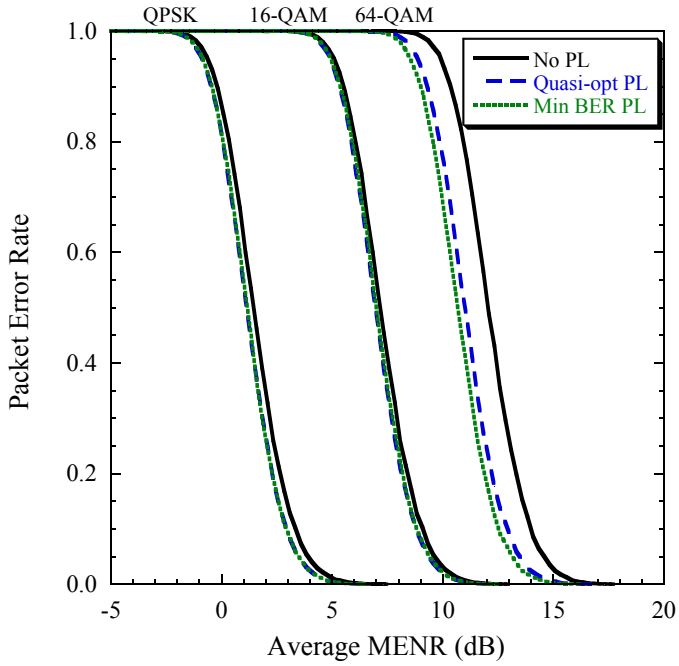

Figure 3.5: Packet error rate for different power loading algorithms and modulation formats, using the rate 0.495 code, $\mathcal{N} = 16$ subcarriers.

later in Chapter 5. However, it should be noted that a protocol with adaptive coding but a fixed modulation is relatively simple to implement. The PSI-N protocol is given perfect channel state information and always chooses the code rate and subcarrier modulation formats that maximize the expected throughput for the channel for each transmission. A final curve labeled as adaptive modulation and coding with no CSI and no power loading is also shown. This represents an older version of the adaptive modulation and coding protocol given later, which has slightly lower performance than what is presented in the next chapters.

The average throughput of 16-QAM with the rate 0.495 code is low because it cannot switch to a more robust code when subchannel conditions are poor, and it likewise cannot switch to a higher-rate code when so much redundancy is unnecessary. Other fixed combinations of modulations used with a fixed code rate, such as QPSK with a higher or

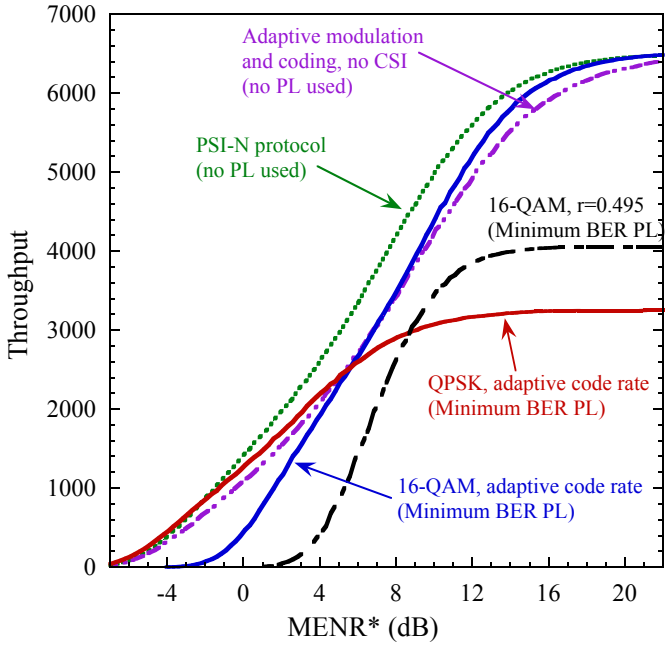

Figure 3.6: Throughput for adaptive modulation and coding algorithms versus power loading with adaptive coding, Rayleigh fading channel, $\mathcal{N} = 4$ subcarriers.

lower-rate code (not shown), also perform poorly compared to the adaptive coding schemes, no matter which of the power loading schemes discussed are used. Despite being given perfect CSI, there is not much the power loading algorithms can contribute. The adaptive modulation and coding protocol without CSI consistently outperforms static modulation and coding using power loading with perfect CSI over the range of MENR of interest.

Although power loading can vastly improve the uncoded bit error rate of OFDM systems subject to frequency-selective fading in high signal-to-noise ratio conditions, it does not improve the performance nearly as significantly for OFDM with error-control coding. Furthermore, the power loading techniques investigated here require perfect channel state information, and they have high computational complexity that is unsuitable for real-time application. Although suboptimal power loading schemes to reduce computational complexity may be able to operate with more limited channel state information,

reduced feedback, and lower computational cost, they do not contribute much considering the limited advantages yielded by power loading algorithms without such constraints.

Chapter 4

Simplified subcarrier ordering for OFDM

One of the key concerns in the previous chapter for power loading and also for other adaptive transmission techniques for OFDM is the stipulation of having good channel state information to guide the selection of transmission parameters from packet to packet. This chapter develops and evaluates a technique, which does not rely on traditional channel measurements, for ordering subcarriers by estimated subchannel quality. This ordering can then be exploited for adaptive modulation adaptation in Chapter 5.

First comes the description of the subcarrier ordering procedure and the statistics it relies on in Section 4.1. Three statistics based on subcarrier error counts are introduced as possibilities to use for ordering the subcarriers. Then those methods are evaluated in Section 4.2. Finally, the ordering techniques are compared with traditional channel measurements in Section 4.3, which includes discussions on the limitations of such measurements.

4.1 Subcarrier ordering procedure

To order subchannels by quality, we need some way to identify which subchannels have better conditions than others. Rather than rely on direct channel gain estimation,

we examine the decoding process at the receiver for an alternative. After each successful packet transmission, the receiver can determine the *subcarrier error count* (SEC) [24], the number of hard decision errors that occurred over a given subchannel for that transmission. Note that this statistic counts the number of errors that would have occurred if there were no error-control coding; in reality, the channel outputs are fed to a (quantized) iterative soft-decision decoder.

The SEC can be determined by simply comparing the demodulator outputs to the original binary code symbols that were transmitted, which themselves can be determined by re-encoding the information bits. We denote the SEC for subcarrier i and packet t as X_i^t. For all such superscripts as the t in X_i^t in this thesis, the superscript should be interpreted as a designation of which packet is in question, not an operation of exponentiation.

Our goal is to order the subcarriers in order of estimated quality, giving each a number from 1 to $\mathcal{N}$. Rank $r_j^t = 1$ indicates that subcarrier j has the best estimated conditions for packet t, while rank $r_k^t = \mathcal{N}$ indicates that subcarrier k is the worst, with the others falling between those extremes.

However, when the subcarrier modulation formats are not all the same, then the error counts for each subcarrier are not directly comparable. First of all, the number of modulation symbols is the same for each subcarrier in a packet, but a higher-order modulation format carries more code symbols per modulation symbol so the total number of code symbols for each subcarrier differs. Secondly, the probability of an error is different; for QPSK and 16-QAM, the probabilities of binary symbol error are known to be (3.2) and (3.3). Therefore the error count for subcarrier i, denoted by X_i, has approximately the binomial distribution with probability mass function given by

$$\mathrm{P}(X_i = k) \approx \binom{n}{k} (P_{e,i})^k (1 - P_{e,i})^{(n-k)}, \quad k = 0, 1, \ldots, n, \tag{4.1}$$

with parameter $n = 2\mathcal{B}$ for QPSK and $n = 4\mathcal{B}$ for 16-QAM, where $\mathcal{B}$ is the number of transmission blocks per packet. For QPSK, the bit errors are independent, so the above holds with equality. However, if we condition on the event that the packet was successful, the distribution is skewed regardless of the modulation format used. That said, because the probability of packet success is typically high, the approximation in (4.1) is good, even when conditioned on the event that the packet was successful, which is necessary for us to be able to compute the SEC. The transmission block is defined as the collection of all $\mathcal{N}$ modulation symbols, one per subcarrier, being transmitted at any given time. Consequently, the number of transmission blocks for a packet depends on the modulation formats used on the different subcarriers, the total number of information bits, and the error-control code used. Because the subcarrier fade levels and energy to noise-density ratios are unknown, the distribution of X_i^t is unknown for each subcarrier.

What we would like is a statistic that is directly comparable between subcarriers using different modulation formats: one that is lower for lower SNR and higher for higher SNR. Therefore, we define a new statistic for each subcarrier i and packet t as

$$\hat{X}_i^t = \begin{cases} 2\,\alpha\, X_i^t, & M_i^t = 2, \\ X_i^t, & M_i^t = 4, \end{cases} \tag{4.2}$$

where M_i^t is the index for the subcarrier modulation format for packet t and subcarrier i. It is 2 for QPSK and 4 for 16-QAM. We select α as a scale factor to roughly account for the discrepancy in bit error rates between the two modulation formats, while the 2 is used to compensate for the fact that there are twice as many code symbols per 16-QAM modulation symbol than there are per QPSK modulation symbol: $4\mathcal{B}$ as compared to $2\mathcal{B}$. The value of α can be optimized for the range of SNR of greatest interest; for a given MENR, it is simple to choose α such that the expected value of αX_i^t for QPSK is equal to that of X_i^t

MENR_i (dB)	$\text{MENR}_j = \text{MENR}_i - 2$ (dB)		$\text{MENR}_j = \text{MENR}_i - 4$ (dB)	
	$P(X_i > X_j)$	$P(X_i = X_j)$	$P(X_i > X_j)$	$P(X_i = X_j)$
0	0.1800	0.0661	0.0565	0.0295
2	0.1459	0.0691	0.0322	0.0224
4	0.1209	0.0808	0.0188	0.0189
6	0.1077	0.1183	0.0137	0.0224
8	0.0933	0.2561	0.0144	0.0510
10	0.0336	0.6595	0.0114	0.2309
12	0.0021	0.9491	0.0015	0.6792

Table 4.1: Error count probabilities for subcarriers i and j, QPSK modulation and $\mathcal{B} = 32$ transmission blocks.

for 16-QAM, for example. Other criteria can be selected, and this could also be extended to a greater number of modulation formats by using multiple scaling factors. Note that if α is made large enough, then a single error or more on a subcarrier using a lower-order modulation is considered worse than any number of errors on a higher-order modulation.

The normalized SEC is discrete, and the distribution depends on the subcarrier MENR as well as the number of transmission blocks $\mathcal{B}$ per packet. From (3.2), (3.3), and (4.1), the probabilities that two subchannels i and j with conditions on i being better than conditions on j and the error count on i being greater or equal to the error count on j for a transmission can be readily calculated. Those probabilities are shown in Table 4.1 for $\mathcal{B} = 32$, for different values of MENR_i and MENR_j. As the SNRs increase, $P(X_i = X_j)$ grows larger, primarily because it is likely for both statistics to be 0. With $\mathcal{B} = 128$ transmission blocks, the probabilities are smaller. For example, for $\mathcal{B} = 32$ with $\text{MENR}_i = 8$ dB and $\text{MENR}_j = 4$ dB, $P(X_i > X_j)$ and $P(X_i = X_j)$ are 0.0144 and 0.0510 respectively; for $\mathcal{B} = 128$ and the same SNRs, those probabilities drop to 6.1×10^{-5} and 1.5×10^{-4}. Thus, we expect that error count-based ordering should be more effective when longer packets are used, as long as the channel does not change so rapidly that the information is already outdated by the time of the next transmission.

If the coherence time of the fading channel is relatively large compared to packet durations, subchannel conditions for consecutive transmissions should be highly correlated. In this case, using statistic values from multiple previous packets will usually improve ordering performance. We examine the performance of the normalized SEC ordering and two variants: SEC ordering that resolves ties (SEC-RT) and SEC ordering with a weighted average (SEC-WA). All of these are based on the normalized SEC in the form of $\hat{X}_i^t$ as described above.

For SEC ordering, $\hat{X}_i^t$ is directly applied and compared between subcarriers. The SEC-RT behaves the same way except in the cases where $\hat{X}_i^t = \hat{X}_j^t$ for two different subcarriers i and j. Then $\hat{X}_i^{t-1}$ is compared with $\hat{X}_j^{t-1}$. If there is again a tie (and again), the statistics for transmission $t-2$ (and $t-3$ as necessary) are compared. As such, we say the SEC-RT resolves ties using the history of the last four packet transmissions. Finally, the SEC-WA ordering takes a weighted average of the last four metric values: $\sum_{k=0}^{3} 2^{-k}\hat{X}_i^{t-k}$. Here, 2^{-k} should be interpreted as 2 to the power of $-k$, whereas the superscript on $\hat{X}_i^{t-k}$ simply refers to packet number $t-k$, as it does in all other cases where the superscript is used in the thesis.

For any of these ordering procedures, if there is still a tie in statistic value between two or more subcarriers, then the subcarrier using the higher-order modulation format is considered to have better subchannel conditions. If both subcarriers used the same modulation format, then the tie is broken randomly with equal probability for each order. Finally, we note that some previous transmissions prior to t may have ended in failure. When that occurs the error counts cannot be calculated, so $\hat{X}_i^{\tau}$ for a failed transmission τ is 0 for each subcarrier.

4.2 Subcarrier ordering evaluation

Ideally, a subcarrier ordering procedure would be able to sort the subchannels perfectly in terms of channel quality. However, any system relying on imperfect channel state information or metrics may not produce the optimal ranking. To understand which ordering algorithms perform better than others, we devise an ordering error statistic to allow for quantitative comparisons.

We define the *ordering error* for any two pairs of subcarriers i and j to be

$$e(i,j) = \begin{cases} \eta_i^t - \eta_j^t, & r_i^t > r_j^t \text{ and } \eta_i^t > \eta_j^t \\ \eta_j^t - \eta_i^t, & r_i^t < r_j^t \text{ and } \eta_i^t < \eta_j^t \\ 0, & \text{otherwise,} \end{cases} \tag{4.3}$$

where η_i^t is the signal-to-interference-plus-noise ratio (in dB) for for subcarrier i and packet t. For each subcarrier (dropping for now the subscript i and superscript t denoting the subcarrier and packet), $\eta = 10\log_{10}\{\mathscr{E}_m/(\mathscr{E}_\iota + N_0)\}$, where $\mathscr{E}_m$ represents the average modulation symbol energy for the desired signal and $\mathscr{E}_\iota$ is the same for the interference signal. When there is no interference, $\mathscr{E}_\iota = 0$ and this expression reduces to the MENR for that subcarrier and packet transmission. The *average ordering error* is then the average over all unique pairs of subcarriers,

$$E_p = \binom{N}{2}^{-1} \sum_{(i,j),i>j} e(i,j). \tag{4.4}$$

The packet average ordering is evaluated for different channels through Monte Carlo simulation for an adaptive modulation and coding system on Nakagami-m fading channels modeled as described in Section 2.1. Our objective at this point is simply to determine the average ordering errors. Therefore, we only consider an idealized adaptation

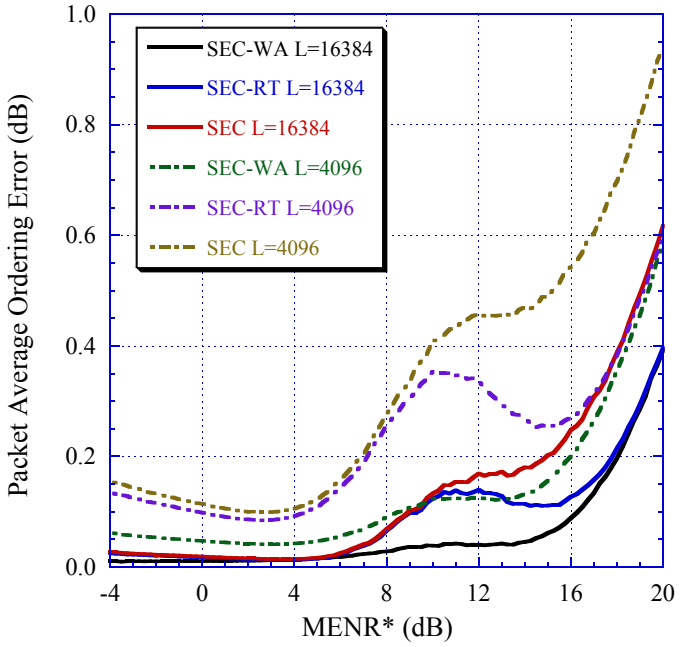

Figure 4.1: Average ordering error for Rayleigh fading channel, $f_d T_s = 0.020$, $\mathcal{G} = 4$ groups, α large.

algorithm that always uses the subcarrier modulation formats and code rates that maximize the throughput over the channel, though any procedure that would choose realistic transmission parameters would be sufficient for our purposes here. This allows for a wide range of channel conditions and modulation format combinations to be tested. For example, in some all the subcarriers may have similar conditions, while in others different subcarriers may experience much more severe fading than others.

The average ordering for the SEC, SEC-RT, and SEC-WA ranking algorithms is presented in Fig. 4.1 for two different packet lengths. The packet length L is the number of binary code symbols per transmission; thus, the number of information bits delivered per successful packet depends on the code rate. For the channel considered, the SEC-WA ordering outperforms the SEC-RT ordering, which in turn is superior to the simple SEC ordering. In a more dynamic channel with quickly changing conditions from interference,

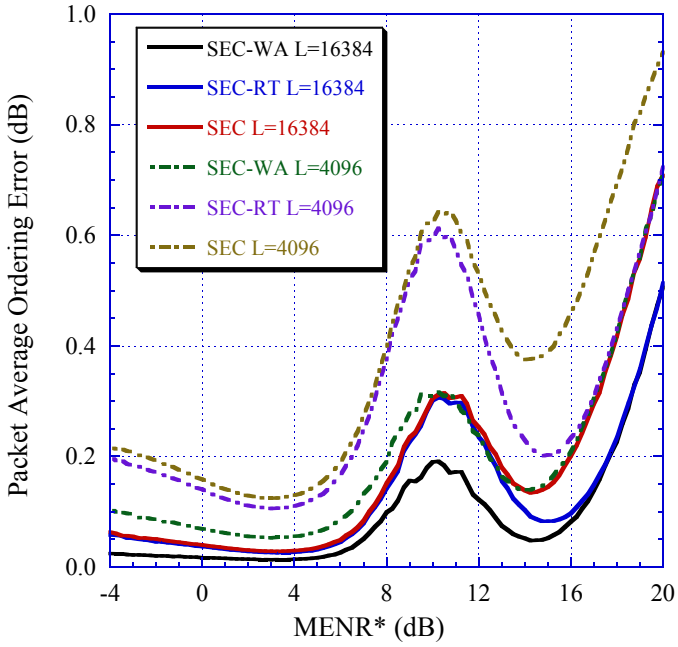

Figure 4.2: Average ordering error for Nakagami-m fading with $m = 2.5$, $f_d T_s = 0.020$, $\mathcal{G} = 4$ groups, α large.

fading, or some other source, the SEC-WA and SEC-RT may be considering error counts from channel conditions that are no longer relevant. Thus, in real channels the SEC-RT and especially SEC-WA could possibly perform relatively worse. Also, from Fig. 4.1 it is clear that longer packet lengths result in better ordering performance.

The average ordering error increases from MENR* = 4 dB to around MENR* = 12 dB because this is the region where a mixture of QPSK and 16-QAM modulation formats is selected with high probability. When there are more subcarriers using different modulation formats, the ordering becomes more difficult, as explained previously. Finally, the ordering error increases further at MENR* above 16 dB because for very high SNR, the subcarrier error counts are frequently zero, even for relatively poorer subchannel conditions, making the subchannels less distinguishable. Note that the SEC and SEC-RT produce similar ordering performance except at high SNR. This is because the SEC-RT can often resolve ties

between multiple subcarriers with an SEC of 0. The increased ordering error at higher SNR can also be seen in Fig. 4.2 for the Nakagami-m channel with $m = 2.5$.

However, the high SNR regime is not of much interest for many applications, including adaptive modulation. In that region, all subcarriers would use the highest-order modulation format possible anyway, so there is no need to determine which subcarrier has excellent rather than very good conditions. If higher potential throughput or higher ordering accuracy at higher SNR are of interest, then the system might include a higher-order modulation format. With a higher-order modulation formats used on some subcarriers, the SECs would be higher, which would result in better ordering performance. In other words, SEC-based ordering works well so long as we restrict attention to ranges of SNR of practical interest.

Different channel fading parameters were also simulated and evaluated, but for brevity and because the results are so similar, they are not shown here. With slower fading (lower normalized Doppler frequency) or Nakagami-m fading with a higher value of the m parameter, the packet average ordering error decreases. Under these conditions, it is even more favorable to use SEC-based ordering techniques to determine the relative subchannel qualities.

4.3 Comparison with subcarrier measurements

Traditional subchannel estimation techniques for OFDM rely on channel measurements to determine the received signal power on each of the subcarriers. Often, these are made from known pilot symbols that are spread across the subcarriers and typically transmitted regularly in time such that the channel estimates can be regularly updated [25–27]. Accuracy depends on the quality of the measurements and may rely on assumptions about the channel conditions and correlation across subcarriers. In some schemes, channel esti-

mates are taken at different frequencies and need to be interpolated across the subcarriers. This necessitates that subcarriers be spaced close together in frequency, which would create additional complexity for systems utilizing multiple frequency bands or only transmitting on a select number of subcarriers within a frequency band.

Furthermore, channel gain measurements can be oblivious the effects of interference. Interference increases the received energy on affected subcarriers compared to having no interference, but this decreases rather than increases the link quality, making successful decoding less likely. On the other hand, if interference is present, this increases the probabilities of bit error and thus the expected SEC and normalized SEC-based metrics for each subcarrier. Subcarriers subject to more severe fading experience worse degradation and are more likely to have a higher SEC, given equivalent fading. Other deviations from ideal operation from sources such as amplifier nonlinearities and imperfect phase synchronization may not be accounted for by channel gain measurements but can degrade the performance of subcarriers, causing higher SEC. As such, the SEC is sensitive to degradations in channel conditions that are not detected by the usual channel measurements, which is a desirable property.

In general, the specifics of the channel measurement scheme and the channel fading dictate the accuracy of the estimated subchannel gain levels. For the purposes of comparison with our SEC-based ordering error techniques, we assume the channel measurements to be perfect other than an error term $Y_i^{(t)}$ for each subcarrier i and packet t that can be modeled as a zero-mean random variable in dB. Each $Y_i^{(t)}$ is independent. The standard deviation of the random variable is given as σ. The system uses the "noisy" subchannel measurements to order the subcarriers by quality, rather than any procedure based on error counts. Here it is assumed that there is no interference.

With these assumptions, the average ordering error based on channel measurements is shown in Fig. 4.3 for various values of m as a function of the estimation error standard

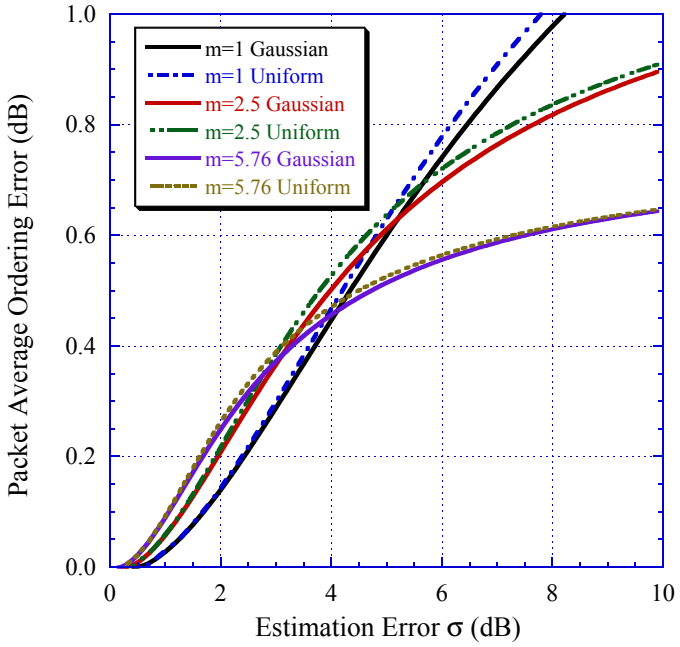

Figure 4.3: Average ordering error for perfect ordering based on channel measurements, $\mathcal{N} = 64$ subcarriers, $\mathcal{G} = 4$ groups, $f_d T_s = 0.020$.

deviation σ. The measurement error does not depend on the packet length L for this model of subchannel measurement error. The error given for various values of σ and for both Gaussian and uniform distributions for each $Y_i^{(t)}$. As can be seen, there is not much difference in the ordering error between when Gaussian and uniform distributions are assumed, so the remainder of the results given in this section will simply be for the Gaussian distribution. As expected, the average ordering error increases as the measurement error increases. Also, as m increases the differences between the fade levels decreases for the subcarriers, which has the effect of decreasing the error terms in (4.3) whenever there is an error, which seems to be the primary effect at very large values of σ. However, with higher m the fade levels being more similar also makes ordering errors more likely to occur.

The average ordering error using SEC-based techniques and channel measurements is given in Figs. 4.4 and 4.5 for m=1 and m=2.5 respectively, now as a function of MENR*.

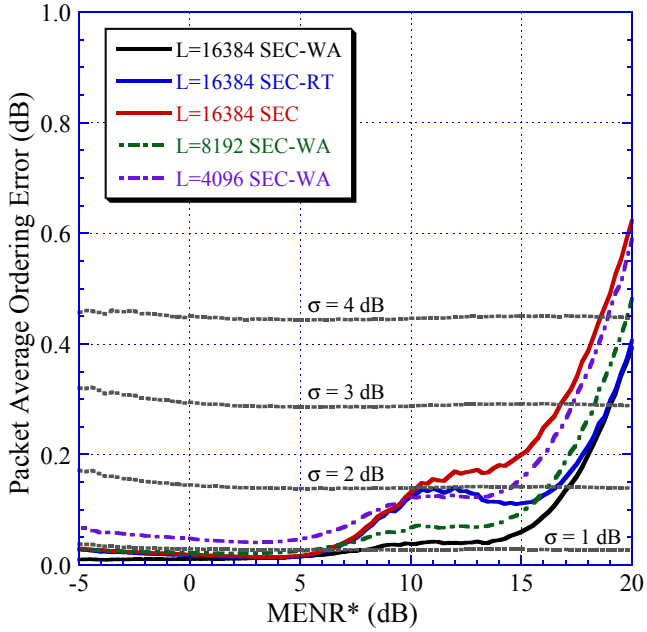

Figure 4.4: Average ordering error, $\mathcal{N} = 64$ subcarriers, $\mathcal{G} = 4$ groups, $m = 1$, $f_d T_s = 0.020$.

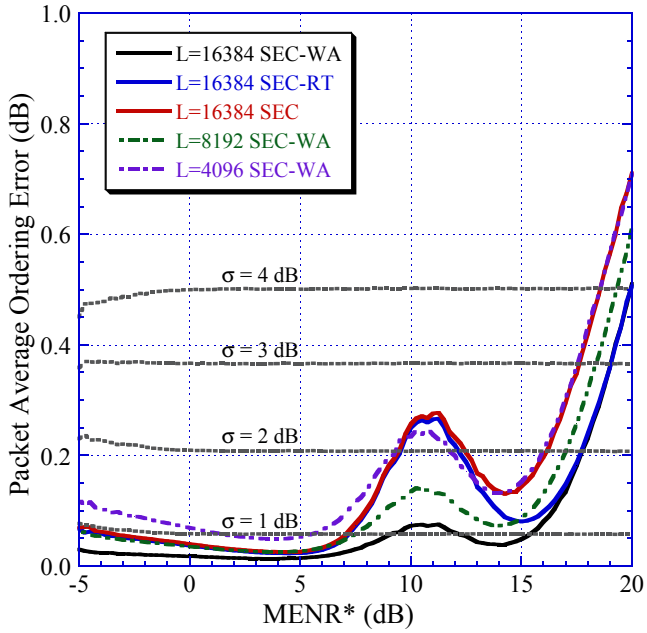

Figure 4.5: Average ordering error, $\mathcal{N} = 64$ subcarriers, $\mathcal{G} = 4$ groups, $m = 2.5$, $f_d T_s = 0.020$.

The ordering error for channel measurements is plotted for multiple values of σ. The SEC-WA ordering for the longer packet length of $L = 16384$ produces a similar or better error as the direct channel measurements for $\sigma = 1$ dB for both cases across much of the range of MENR*. The SEC-WA for the shorter packet lengths as well as the SEC-RT and SEC for $L = 16384$ are competitive with or better performing than the channel measurements for $\sigma = 2$ dB again until high MENR* around 15 dB and higher.

Now, as a simple example demonstrating the problems channel measurement techniques may face with interference, consider the average ordering error when all subcarriers use QPSK and the rate 0.495 code is always used. Suppose that half of the $\mathcal{N}$ subchannels as seen by the receiver are subject to interference in the form of an interfering transmission also using QPSK. For this example, we assume that the interfering transmission is phase aligned with the desired transmission that is being received but the polarity is generated independently of the desired transmission, so the interference can add constructively or destructively each with probability 0.5. The interfering signal has a power 6 dB less than the primary signal at the receiver and is always present. As can be seen in Fig. 4.6, the SEC-based ordering is robust against this significant amount of interference. The average ordering error is increased by less than 0.05 dB for SEC-WA except until MENR* above 12 dB, with the difference usually being less than that.

For the channel measurements, we assume that the signal level is measured the same way as it was done without interference and furthermore that the interference does not even impact the subchannel measurements. The interfering signal could well induce additional measurement error in practice. For example, the interference could add to signal levels during the measurements and convince the receiver that the channel is better when in fact the interference is degrading the performance at that frequency. The performance for the channel measurements is plotted and compared with the SEC-WA and SEC in Fig. 4.7. Even at the small packet size of $L = 4096$, the SEC ordering (even without any weighted

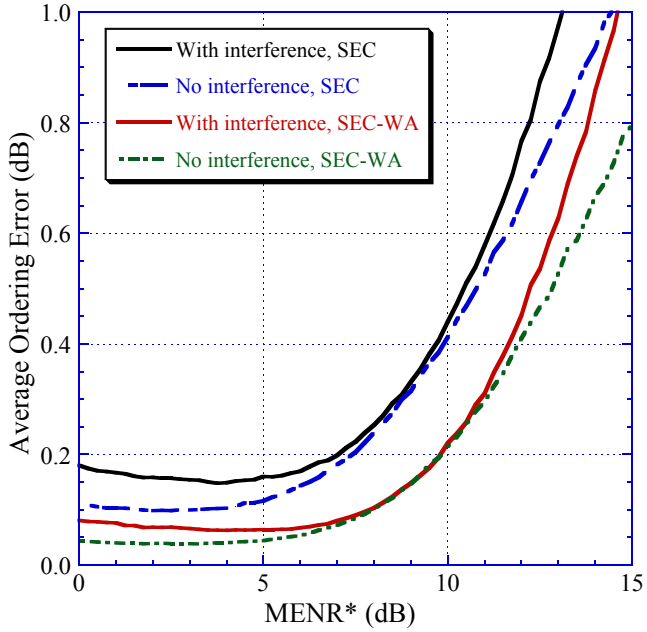

Figure 4.6: Average ordering error for fixed QPSK and 0.495 code rate, SEC and SEC-WA ordering, with and without interference, $L = 4096$, $\mathcal{N} = 64$ subcarriers, $\mathcal{G} = 4$ groups, $m = 1$, $f_d T_s = 0.020$.

average) outperforms the measurement approach even at $\sigma = 0$ dB. The performance of the SEC-based ordering at larger packet sizes (not shown) improves as it does without interference, so the difference with the measurement approach increases in that case.

The reason the average ordering error using channel measurements increases with MENR* is because the interference level is assumed to be 6 dB less than the signal level, so this interference term dominates the noise at high MENR*. Results not shown indicate similar trends for different stipulations on the interfering signal and smaller interference levels, so the limitations of subchannel measurement-based ordering are seen across a range of channels and are not limited to the example shown. Thus, subcarrier ordering using the SEC, SEC-RT, and SEC-WA is cheaper than implementations relying on subchannel measurements, and it may also outperform them for wireless channels of practical interest. The SEC is an indicator of any perturbance in the channel or system produces conditions

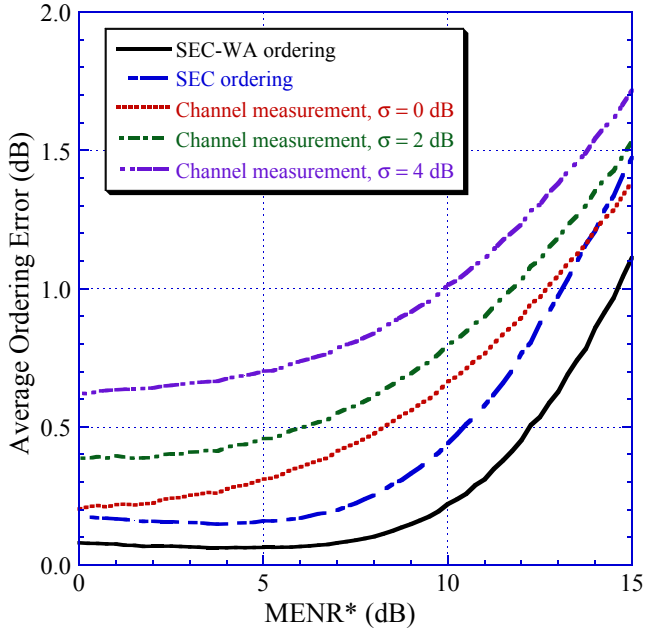

Figure 4.7: Average ordering error for fixed QPSK and 0.495 code rate, SEC-based ordering ordering compared against ordering from SNR measurements, with and without interference, $L = 4096$, $\mathcal{N} = 64$ subcarriers, $\mathcal{G} = 4$ groups, $m = 1$, $f_d T_s = 0.020$.

that make decoding less likely to succeed, so it is a robust measure of channel quality.

Chapter 5

Adaptive modulation and coding protocol

This chapter details an adaptive modulation and coding protocol that is based on the subcarrier error count (SEC) introduced in Chapter 4. It was shown in Chapter 3 that adaptive power loading has limited use for OFDM communications systems of interest that use forward error correction codes. Here the focus instead is on making the most of per-subcarrier adaptive modulation and then selecting a suitable code rate to improve the performance over the channel as conditions change. Although it is clear that subcarriers with worse estimated channel conditions should not be using higher-order modulation formats than those with better estimated channel conditions, the exact modulation format selection process needs to be developed.

First, an overview of the goals and structure of the adaptive adaptive modulation and coding protocol is given in Section 5.1. This is followed by details of the code adaptation and modulation adaptation processes in Sections 5.2 and 5.3 respectively. A framework and points of reference needed to evaluate the adaptive protocol are the subject of Section 5.4. Idealized perfect state information protocols describe a ceiling on performance achievable by any adaptive protocol. Finally, the performance results and comparisons for the adaptive modulation and coding protocol appear in Section 5.5.

5.1 Adaptive protocol overview

The goal of our *adaptive modulation and coding protocol* (AMCP) is to maximize the performance a communications session over the fading channel by changing the error-control code and individual subcarrier modulation formats from packet to packet as subchannel conditions change. Consequently, the performance measure of choice is the session throughput and not the packet or bit error rate, which would be optimized by choosing lower-rate codes and modulation formats even when the subchannel conditions are favorable. Specifically, we examine the average throughput achieved over a communications session in which one transmitter sends packets to one receiver. The session throughput is defined to be the total number of information bits successfully received divided by the total time spent transmitting. Only information bits in packets that are successfully decoded count towards the term in the numerator, while all time spent transmitting counts towards the term in the denominator, regardless of whether the packets can be decoded. For consistency with previous results, session throughput is normalized and represented as the number of information bits delivered per time unit, which is set as the duration of 32 OFDM blocks.

Essentially, we need to map $\mathcal{N}$ subcarrier modulation formats and one code to the $\mathcal{N}$ subchannel states. One strategy would be to treat the SECs as crude signal-to-noise ratio estimators and use these to track all $\mathcal{N}$ subchannel states as they vary from packet to packet. However, the SEC and even the SEC-WA statistic provides a poor estimate of exact channel conditions, particularly if the number of binary code symbols per subcarrier per transmission is not high. Furthermore, even if all the subchannel conditions were given, the subcarrier modulation formats and error-control code that maximize the session throughput over a particular channel are unknown. The hard-decision error rate can be computed, but its relationship with the packet error rate is unclear and intractable, because

all $\mathcal{N}$ subcarriers contribute soft-decision inputs to the iterative decoder.

Just as the subcarrier error counts can be used to order subchannels by quality, they can also help determine the overall channel quality across all the subcarriers. Our proposed adaptive protocol selects modulation formats and the code rate based on the *total error rate* (TER) and then leverages the subcarrier ordering procedures described in Chapter 4 to assign those modulation formats to the subcarriers. The TER is defined as the number of hard-decision errors at the demodulator output for one packet divided by the total number of binary code symbols. Like the subcarrier error count, this can only be determined if the packet is decoded correctly. The TER can be calculated by summing all of the SECs (before normalization) and dividing that sum by the number of binary code symbols in the packet. Unlike for the SECs, for which it can be beneficial to examine the statistics from multiple previous transmissions, there is already a large enough sample size of binary code symbols across all $\mathcal{N}$ subcarriers generating the TER, so we only look at the TER for the most recent packet transmission.

Thus, all of channel information necessary to operate the adaptive protocol is generated via the error counts and information already known to the system such as the modulation formats used for prior transmissions. The protocol does not require any direct channel measurements. However, the error counts are computed at the receiver, not the transmitter in the system. In order for the transmitter to learn which modulation formats and code rate are appropriate for the next transmission, there are two possibilities. In the first, the receiver reports the TER and estimated subcarrier order back to the transmitter, and the transmitter is responsible for the adaptive protocol procedures described in the next sections. The other method would be for the receiver to run the logic of the adaptive protocol and simply report back which modulation formats and code rate should be used. Either way, the required feedback can be sent to the transmitter in regular acknowledgment packets, which typically are sent with a more robust modulation and coding and should be received. For

this thesis we assume that the feedback information is always available after a successful transmission.

The overall strategy for the adaptive protocol is to adjust the transmission parameters incrementally based on prior transmission parameters. For the transmission of packet number $t+1$ in a communications session, information is needed about the error counts, code, and modulation formats for the previous packet, t. We denote C^t as the index for the code used for packet t and M_i^t as the index for modulation format for the subcarrier i on packet t. A higher code index denotes a higher-rate code, with an index of 1 representing the lowest-rate code. Recall that there are five turbo product codes of rates 0.236, 0.325, 0.495, 0.660, and 0.793, so valid code indices range from 1 to 5. The modulation index for QPSK is 2, while the index for 16-QAM is 4, representing the number of binary code symbols per modulation symbol for each.

We denote the code-modulation assignment for a given packet as $(C, \mathbf{M})$, dropping for now the superscripts representing the packet number, where the modulation format indices for all $\mathcal{N}$ subcarriers is given by $\mathbf{M}$. As just mentioned, C represents the code index. Supposing there are κ available codes and M modulation formats on each of $\mathcal{N}$ subcarriers, there are $\kappa \times M^{\mathcal{N}}$ possible code-modulation assignments. This turns out to be 5×2^{64} for the system considered for the numerical evaluations.

5.2 Code adaptation

The first step of the adaptive protocol is selecting the code rate. Upon successful packet decoding of transmission t, we compute the TER, which gives information about the channel quality and roughly how close the previous transmission was to decoding incorrectly. However, in the case that the packet actually fails to decode, we need a fallback

mechanism. In that case the code to be used for the next transmission is chosen to be

$$C^{t+1} = \begin{cases} C^t - 1, & C^t > 1 \\ 1, & C^t = 1. \end{cases} \tag{5.1}$$

In other words, the code with the next lowest rate is used if it exists. This reduces increases the probability that the next transmission will be successful, whereupon the protocol can return to using the TER statistic. If the failed transmission was already using the lowest-rate code, then then all subcarriers switch to a lower-rate modulation format (if available), which produces a similar effect. Following this step-down procedure, a transmission should succeed eventually unless the channel has become so poor that any communications is impossible. Perhaps as a last resort, the total transmission power could be increased, but how and when to increase the transmission power is beyond the scope of this thesis. For our analyses we assume that a suitable transmission power has been set at the start of the session, and it cannot be adjusted afterwards. The rest of the section describes the procedure when packet $t-1$ was decoded correctly.

Let $\mathcal{R}^t$ be the TER for packet t. If $\mathcal{R}^t$ falls in the interval $(\gamma_{k,1}, \gamma_{k,2}]$, then code index k is used for the next transmission. The codes and other corresponding thresholds are listed in Table 5.1. If a packet transmission resulted in a low total error count, this means that less redundancy is required, so a code with a higher rate may be used for the next transmission, increasing the potential throughput. On the other hand, a high TER means that a lower-rate code with a higher probability of decoding success should be used. Note that this provides a mechanism for the protocol to switch to a lower-rate code even when there are yet no packet errors. By doing so, we can avoid future packet failures. On the other hand, the TER can also indicate that the subchannels overall have improved significantly, allowing the code to be adapted in the case that less redundancy is required.

Code Index (k)	Code Rate	$\gamma_{k,1}$	$\gamma_{k,2}$
1	0.236	0.167	1.000
2	0.325	0.112	0.167
3	0.495	0.059	0.112
4	0.660	0.038	0.059
5	0.793	0.000	0.038

Table 5.1: Endpoints for the code adaptation interval tests.

However, there is no set of code adaptation endpoints that is optimal in every possible channel. Though the TER gives information about the performance over the channel for the previous transmission, it is possible that the subchannel fading could be significantly different for the next transmission, and we do not assume knowledge of the statistical distributions of the channels. Furthermore, systems may be deployed in a situation where they may encounter a variety of fading channel conditions. Thus, the endpoints in Table 5.1 were chosen based on many simulation results to perform well across a wide variety of channels. Because of the iterative soft-decision decoding, there is no direct relationship between the TER and packet errors for any code, but worse channel conditions and higher-order modulations do result in higher TERs and higher probabilities of packet failure. The relationship between the TER and the packet error rate is given in Fig. 5.1 for packets of length $L = 4096$. The graph shows the packet error rate determined through simulation as a function of TER for the five codes considered.

If the thresholds $\gamma_{k,1}$ and $\gamma_{k,2}$ are too high, then the protocol does not choose the higher-rate codes in situations it should, so the unnecessary redundancy lowers the session throughput. If the values are too low, then the protocol chooses higher-rate codes too frequently, resulting in excessive failed transmissions that also lower session throughput. However, the adaptive protocol performance is not sensitive to small differences in the thresholds, so in general it is not necessary to find the optimal values to maintain good performance. When the non-zero and non-unity values of $\gamma_{k,1}$ and $\gamma_{k,1}$ are shifted to be

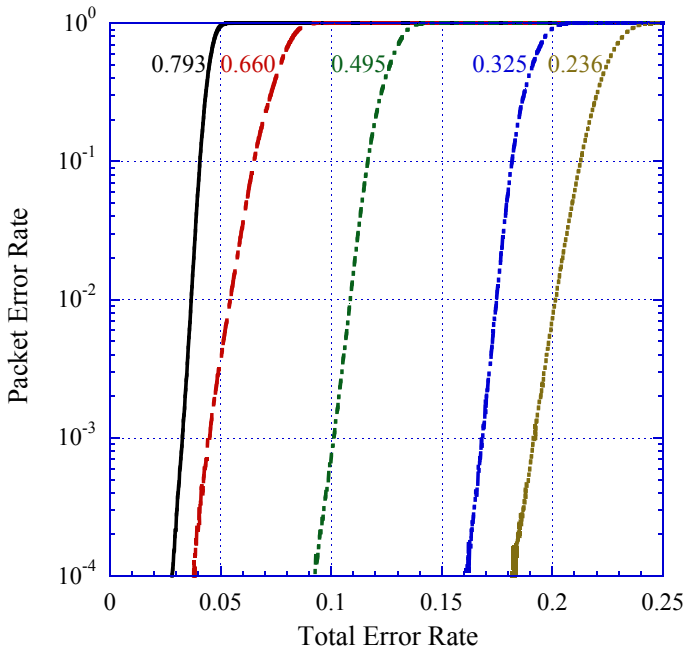

Figure 5.1: Empirical packet error rate at different values of the total error count and code rates, averaged over different channel conditions.

10% higher than shown in Table 5.1, the session throughput seen over the Rayleigh channel decreases by an average of 1.1% compared to using the values in the table. Likewise, if $\gamma_{k,1}$ and $\gamma_{k,1}$ are shifted to be 10% lower than as shown in the table, the session throughput under the same conditions decreases by an average of 0.98%. The average is taken over a range of values of MENR* from 0 dB to 20 dB, and the greatest difference seen between the "correct" values and altered values at any value of MENR* is 5.1%, which occurs for MENR$^* = 3.5$ dB when $\gamma_{k,1}$ and $\gamma_{k,1}$ are lowered by 10%. Hence, the adaptive protocol does not rely on precise fine-tuning of adaptation code adaptation parameters to achieve good performance.

5.3 Modulation adaptation

Because there is only one code used across all subcarriers but a choice of modulation for each single subcarrier, the modulation adaptation part of the adaptive protocol is more complicated than the code adaptation was. In this section we describe a procedure to select between QPSK and 16-QAM modulations. Some future work is required to extend the procedure listed here to a wider range of modulation formats, such as 64-QAM, BPSK, and so on. The TER also plays a critical role in modulation adaptation, but here we also make use of the subcarrier ordering described in Chapter 4. As described previously, the TEC can only be computed upon successful packet reception, so if packet t does not decode successfully, then the fallback strategy depends on the code used for the previous transmission. The modulation format index is

$$M_i^{t+1} = \begin{cases} M_i^t, & C^t > 1 \\ 2, & C^t = 1 \end{cases} \quad \forall \quad i. \tag{5.2}$$

When the previous transmission t is successful, the first step is to determine the modulation formats to use. Specifically, we examine the number of subcarriers each using QPSK and 16-QAM for that transmission. M_4^t is defined as the number of subcarriers to use QPSK, while M_{16}^t is the number of subcarriers to use 16-QAM, each for packet t. In this section, the superscript is dropped whenever for notational convenience when the context is clear. The procedure is to adjust M_4^{t+1} and M_{16}^{t+1} based on the TER. Again, we use another interval test similar to the one used for code rate adaptation. Suppose that the code with index C^t were used for packet t. The same thresholds are used as before from Table 5.1, but this time they are used to create subintervals. If $\mathcal{R}^t$ falls in the interval $(\delta_{j,1}, \delta_{j,2}]$, then the change in modulation formats corresponding to index j is used for the next transmission.

To maximize the session throughput over the channel, there needs to be a careful

balancing of the information rate (upon a successful transmission) and the packet error rates. If the TER is high, we want to use more conservative modulation formats to reduce the probability of packet failure for the next transmission, even though this reduces the information rate of the given transmission. If the TER is low, we wish to use more conservative modulation formats so that even lower TERs can be achieved, whereupon the protocol may switch to a higher-rate code for future transmissions. For TERs falling in between, the change is towards higher-rate modulation formats, which also increases the session throughput so long as the next transmission is successful. The exact changes and intervals for the modulation adaptation are shown in Table 5.2. The values in the table are suitable for $\mathcal{N} = 64$ subcarriers and adaptation between QPSK and 16-QAM. In this case, $M_4^{t+1} = \mathcal{N} - M_{16}^{t+1}$.

There are two exceptions to the procedure described in the table. If the system selected the highest-rate code ($C^{t+1} = 5$) and the TER is less than $1/2\,\gamma_{5,2}$, then the change is $M_{16} := M_{16} + 4$. When already using the highest-rate code, there is no code rate to step up to, so that is why the procedure is different. Also, if M_{16}^{t+1} would be set higher than $\mathcal{N}$, then M_{16}^{t+1} is set to $\mathcal{N}$. Likewise, if M_{16}^{t+1} would be negative, it is set to zero. After all, there cannot be more subcarriers transmitting with any modulation format than there are subcarriers in all.

Once M_4^{t+1} and M_{16}^{t+1} are determined from the above based on the interval test for $\mathcal{R}^t$, it is simply a matter of selecting the M_{16}^{t+1} subcarriers with the best estimated channel conditions to use 16-QAM, while the rest use QPSK. The SEC, SEC-RT, or SEC-WA ordering described in Chapter 4 can then be applied to determine which subcarriers have the best channel conditions, though other methods could also be used. As a comparison, we consider the performance achieved when the adaptive protocol is given the perfect ordering of the subcarriers, rather than ordering based on the subcarrier error counts. The AMCP using this ordering is abbreviated as the AMCP PO, and it represents the best that can be

Index (j)	$\delta_{j,1}$	$\delta_{j,2}$	Change
1	$(1\gamma_{k,1}+7\gamma_{k,2})/8$	∞	$M_{16}^{t+1}=M_{16}^{t}-2$
2	$(2\gamma_{k,1}+6\gamma_{k,2})/8$	$(1\gamma_{k,1}+7\gamma_{k,2})/8$	$M_{16}^{t+1}=M_{16}^{t}-1$
3	$(3\gamma_{k,1}+5\gamma_{k,2})/8$	$(2\gamma_{k,1}+6\gamma_{k,2})/8$	$M_{16}^{t+1}=M_{16}^{t}+2$
4	$(4\gamma_{k,1}+4\gamma_{k,2})/8$	$(3\gamma_{k,1}+5\gamma_{k,2})/8$	$M_{16}^{t+1}=M_{16}^{t}+4$
5	$(5\gamma_{k,1}+3\gamma_{k,2})/8$	$(4\gamma_{k,1}+4\gamma_{k,2})/8$	$M_{16}^{t+1}=M_{16}^{t}+3$
6	$(6\gamma_{k,1}+2\gamma_{k,2})/8$	$(5\gamma_{k,1}+3\gamma_{k,2})/8$	$M_{16}^{t+1}=M_{16}^{t}+2$
7	$(7\gamma_{k,1}+1\gamma_{k,2})/8$	$(6\gamma_{k,1}+2\gamma_{k,2})/8$	$M_{16}^{t+1}=M_{16}^{t}$
8	$\gamma_{k,1}$	$(7\gamma_{k,1}+1\gamma_{k,2})/8$	$M_{16}^{t+1}=M_{16}^{t}-1$
9	$-\infty$	$\gamma_{k,1}$	$M_{16}^{t+1}=M_{16}^{t}$

Table 5.2: Modulation adaptation procedure and endpoints for interval tests.

achieved with any technique for ordering the subcarriers. It is not intended as an alternative to SEC-based ordering techniques, as it is not readily implementable in the real world. Likewise, the AMCP with SEC, SEC-RT, and SEC-WA orderings is denoted as the AMCP SEC, AMCP SEC-RT, and AMCP SEC-WA. The next section describes more benchmarks that can be used as comparisons for the AMCP.

5.4 Performance bounds and analysis

The adaptive protocols proposed in this thesis rely on the SEC and TER to gain information about the channel, using these statistics as a basis for code and modulation adaptation from packet to packet. To evaluate the performance of such methods, which use limited information about the channel, we consider hypothetical protocols that instead are given perfect channel state information. These provide a reference from which the proposed adaptive protocol can be compared. The hypothetical perfect state information protocols require information that will not accurately be known in real-world systems; they are presented here only for benchmark purposes and not as a viable alternative to the proposed adaptive protocol.

The two primary protocols of interest that use perfect information are the Perfect State Information for the Next packet (PSI-N) and Perfect State Information for the preceding packet (PSI-P) protocols. As the name suggests, the PSI-N protocol knows the exact subchannel states for each upcoming transmission, so it represents an idealization of a system that employs channel prediction and estimation, on an idealized wireless channel for which such prediction is possible. The PSI-P is given the exact subchannel states for the for the most recent transmission (regardless of whether or not that packet was successful), which represents the best that a system relying on extensive measurements of the previous packet could achieve. The PSI-P protocol, like the proposed adaptive protocol, uses information about the channel for packet t to select transmission parameters for packet $t+1$. Therefore, the performance should be better when there is higher correlation between channel conditions from one packet to the next, which occurs if the fading is relatively slow.

Furthermore, we assume that the hypothetical protocols also know the exact packet error rates that every assignment of code rate C and subcarrier modulation formats $\mathbf{M}$ achieves for every possible set of subchannel states. These perfect protocols are allowed to choose any code-modulation assignment $(C,\mathbf{M}) \in \mathcal{A}$, where $\mathcal{A}$ is the set containing all assignments of codes and modulation formats, and they use this information to maximize the expected throughput for each transmission. Even if the decoding technique is intractable for analysis, as it is for the system we consider, the packet error rate for each set of potentially most effective code-modulation combinations can still be determined through prior offline simulation.

We note that it will never be advantageous to assign higher-order modulation formats to inferior subchannels, and there must be an integer number of modulation symbols transmitted per packet. For the packet size of 4096 code symbols, there will be 16, 17, and so on all the way to 32 modulation symbols per packet; also, there is no advantage to transmitting with more higher-order modulation formats unless this reduces the total number of

modulation symbols per packet needed. As a result, if the channel states are known, there are only 17 possible combinations of modulation formats and thus 85 code-modulation combinations that must be evaluated offline.

The PSI-N and PSI-P thus have an unrealistic amount of prior information about the channel and the modulation and coding schemes in all forms of fading considered. Another reference point with which to compare the AMCP are protocols that are restricted to using a smaller set of code-modulation assignments such that all subcarriers in any given packet must use the same modulation format. We call these the Restricted PSI-N and Restricted PSI-P protocols. The only difference between the restricted and normal versions is that we now consider code-modulation assignments $(C,\mathbf{M}) \in \mathcal{A}'$, with $\mathcal{A}' \subset \mathcal{A}$, listed in Table 5.3. There are only eight assignments in $\mathcal{A}'$, and for each, every subcarrier uses the same modulation format. Systems using only the restricted set are simpler to implement, so it is worth investigating if the additional performance gained by allowing the full set justifies the additional complexity.

Similarly, the Restricted AMCP is a variant of the AMCP that only uses code-modulation assignments $(C,\mathbf{M}) \in \mathcal{A}'$. Because all the subcarriers use the same modulation format, there is no need for subcarrier ordering, and simply the TER is sufficient for adaptation. The Restricted AMCP choose the code-modulation assignment using an interval test, this time using the values in Table 5.3. However, the details are different than before. If the transmission parameters corresponding to index k are used, then if $\mathcal{R} > \psi_{k,2}$, the next transmission uses index $k-1$ instead. If $\mathcal{R} < \psi_{k,1}$, the switch is to index $k+1$. Otherwise, the protocol selects k again for the next transmission.

Because of the assumptions made about the perfect protocols, it is possible to calculate the session throughput achieved by these with the aid of offline simulation. The

Index	Code Rate	Modulation Format	$\psi_{k,1}$	$\psi_{k,2}$
1	0.236	QPSK	0.179	1.000
2	0.325	QPSK	0.118	0.179
3	0.495	QPSK	0.065	0.118
4	0.660	QPSK	0.040	0.065
5	0.793	QPSK	0.013	0.040
6	0.495	16-QAM	0.071	0.121
7	0.660	16-QAM	0.041	0.071
8	0.793	16-QAM	0.000	0.041

Table 5.3: Combinations of code rate and modulation format in $\mathcal{A}'$ and endpoints for interval tests for Restricted AMCP.

expected session throughput for a packet transmitted during channel state $\mathbf{h}$ is

$$s(C,\mathbf{M}\,|\,\mathbf{h}) = \frac{I_s(C,\mathbf{M}\,|\,\mathbf{h})}{t(\mathbf{M})}, \tag{5.3}$$

where $I_s(C,\mathbf{M}\,|\,\mathbf{h})$ is the average number of information bits successfully delivered per packet transmission with the code and modulation formats specified, for channel state vector $\mathbf{h}$, and $t(\mathbf{M})$ is the duration of a packet transmission. The time $n(\mathbf{M})$ is expressed in terms of time units, which are defined to be the duration of a modulation symbol. To calculate the session throughput achieved by the perfect protocols for any channel, $I_s(C,\mathbf{M}\,|\,\mathbf{h})$ must be determined for all possible channel states $\mathbf{h}$ and transmission parameters C and $\mathbf{M}$. For the system considered here, because of the complexity of the iterative decoding, this requires an extensive set of simulation across a range of channel conditions, which is made possible because of the Markov chain models used for fading.

For each state $\mathbf{j}$ let $(C_\mathbf{j},\mathbf{M}_\mathbf{j}) \in \mathcal{A}$ be the transmission parameters such that $s(C_\mathbf{j},\mathbf{M}_\mathbf{j}) = \max\{s(C,\mathbf{M}) : (C,\mathbf{M}) \in \mathcal{A}\}$. Likewise for the restricted set, let $(C'_\mathbf{j},\mathbf{M}'_\mathbf{j}) \in \mathcal{A}'$ be the transmission parameters such that $s(C'_\mathbf{j},\mathbf{M}'_\mathbf{j}) = \max\{s(C,\mathbf{M}) : (C,\mathbf{M}) \in \mathcal{A}'\}$. Thus over a session, considering the channel states $\mathbf{j}$ out of the possible set $\mathcal{J}$ that are experienced and the steady-state probabilities $\pi_\mathbf{j}$ for each set of states, the expected session throughput achieved by the

PSI-N protocol is

$$\bar{\mathcal{S}}_N = \frac{\sum_{\mathbf{j}\in\mathcal{J}} \pi_{\mathbf{j}} I_s(C_{\mathbf{j}}, \mathbf{M}_{\mathbf{j}} \,|\, \mathbf{j})}{\sum_{\mathbf{j}\in\mathcal{J}} \pi_{\mathbf{j}} t(\mathbf{M}_{\mathbf{j}})}, \tag{5.4}$$

while the Restricted PSI-N protocol achieves

$$\bar{\mathcal{S}}'_N = \frac{\sum_{\mathbf{j}\in\mathcal{J}} \pi_{\mathbf{j}} I_s(C'_{\mathbf{j}}, \mathbf{M}'_{\mathbf{j}} \,|\, \mathbf{j})}{\sum_{\mathbf{j}\in\mathcal{J}} \pi_{\mathbf{j}} t(\mathbf{M}'_{\mathbf{j}})}. \tag{5.5}$$

Similarly, the PSI-P and Restricted PSI-P protocols respectively have session throughputs of

$$\bar{\mathcal{S}}_P = \frac{\sum_{\mathbf{j}\in\mathcal{J}} \pi_{\mathbf{j}} \sum_{\mathbf{h}\in\mathcal{J}} q(\mathbf{h} \,|\, \mathbf{j}) I_s(C_{\mathbf{h}}, \mathbf{M}_{\mathbf{h}} \,|\, \mathbf{j})}{\sum_{\mathbf{j}\in\mathcal{J}} \pi_{\mathbf{j}} t(\mathbf{M}_{\mathbf{j}})} \tag{5.6}$$

and

$$\bar{\mathcal{S}}'_P = \frac{\sum_{\mathbf{j}\in\mathcal{J}} \pi_{\mathbf{j}} \sum_{\mathbf{h}\in\mathcal{J}} q(\mathbf{h} \,|\, \mathbf{j}) I_s(C'_{\mathbf{h}}, \mathbf{M}'_{\mathbf{h}} \,|\, \mathbf{j})}{\sum_{\mathbf{j}\in\mathcal{J}} \pi_{\mathbf{j}} t(\mathbf{M}'_{\mathbf{j}})}. \tag{5.7}$$

The session throughput achieved by the PSI-N and PSI-P protocols under different channel conditions is shown in Fig. 5.2. The PSI-N protocol knows the state of the channel prior to transmission, we assume that channel conditions do not change during a transmission, and the distribution of the fading does not depend on the speed of the fading. Therefore, the results for the PSI-N protocol are the same no matter the speed of the fading. Thus, only one result for the PSI-N protocol for each value of m. The PSI-N protocol has better channel state information than the PSI-P protocol, so it is able to choose more optimal code and modulation formats for each set of subchannel states and thus achieve higher session throughput over most of the range of MENR* shown. As will be seen in all the other performance graphs, at low MENR*, all protocols will select the lowest-order modulation format (QPSK) for all subcarriers and the lowest code rate, so the performance will be the same for all of them. Likewise, at high MENR*, all will select 16-QAM for all subcarriers and the highest code rate, so again the performance will be the same for all algorithms. With slower fading, the PSI-P protocol's information about the channel state

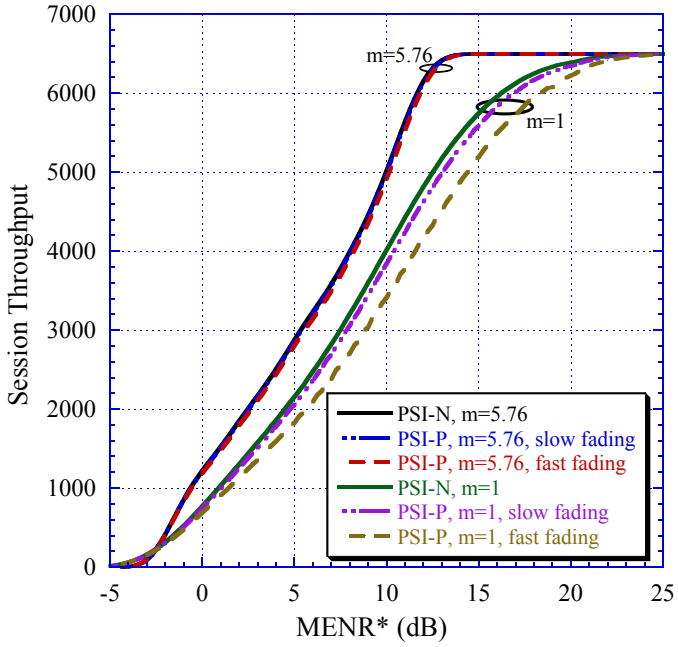

Figure 5.2: Throughput for hypothetical protocols with perfect channel state information, $m = 1$, $\mathcal{N} = 64$ subcarriers, $\mathcal{G} = 4$ groups. Normalized Doppler $f_d T_s$ = 0.005 for slow fading, $f_d T_s$ = 0.020 for fast fading.

is less outdated, so performance is better in slower fading than faster fading. For the lower value of m, the session throughput results for for slow and fast fading diverge more for PSI-P because there is a greater difference in SNR between states and thus lower accuracy of the channel state information.

The session throughputs for the PSI-N and Restricted PSI-N protocols are compared in Fig. 5.3. All the results in this chapter are for the packet length of $L = 4096$; for the larger packet sizes, the throughput is almost identical. Likewise, the same results are shown in Fig. 5.4 for the PSI-P and Restricted PSI-P protocols for the relatively fast fading case (normalized Doppler $f_d T_s = 0.020$). The differences between the full and restricted sets are greater for PSI-N than PSI-P because the PCI-N protocol has even better information about the state of the channel, which it can better exploit when selecting modulation formats on a subcarrier-by-subcarrier basis. In much of the range of interest, where the protocols must

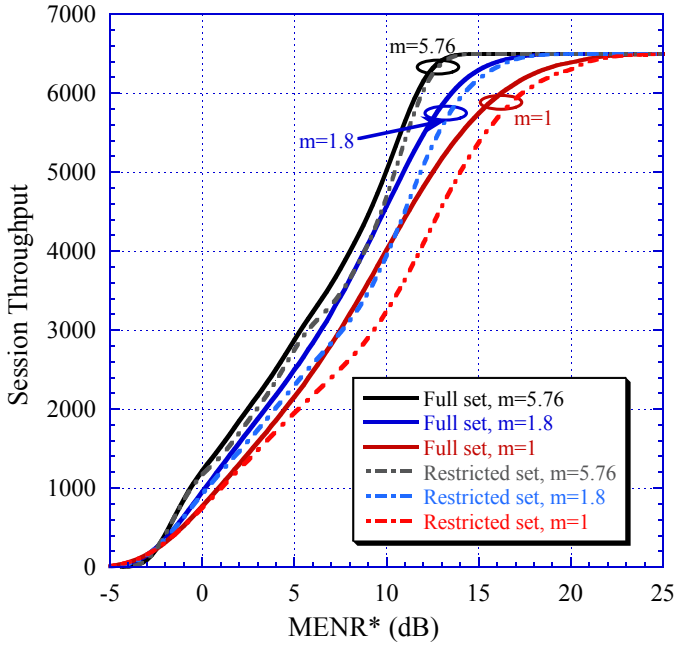

Figure 5.3: Throughput for PSI-N protocol with perfect channel state information, comparing full set $\mathcal{A}$ to restricted set $\mathcal{A}'$, $\mathcal{N} = 64$ subcarriers, $\mathcal{G} = 4$ groups.

adapt between QPSK and 16-QAM modulation, such as around MENR$^* = 10$ dB, the PSI-P protocol with the full set still outperforms the Restricted PSI-P protocol by an average of around 1 to 1.5 dB for $m = 1$, the Rayleigh fading scenario. The further apart the channel conditions are for different subcarriers, the greater the advantage of having per-subcarrier adaptive modulation rather than simply one modulation format for each subcarrier. We also expect the difference to be larger if more modulation formats in addition to QPSK and 16-QAM were available.

5.5 Performance results

Finally, we evaluate the performance of the proposed adaptive modulation and coding protocol. Unlike other schemes proposed in the literature and also the hypothetical perfect state information protocols described in the previous section, it does not rely on any

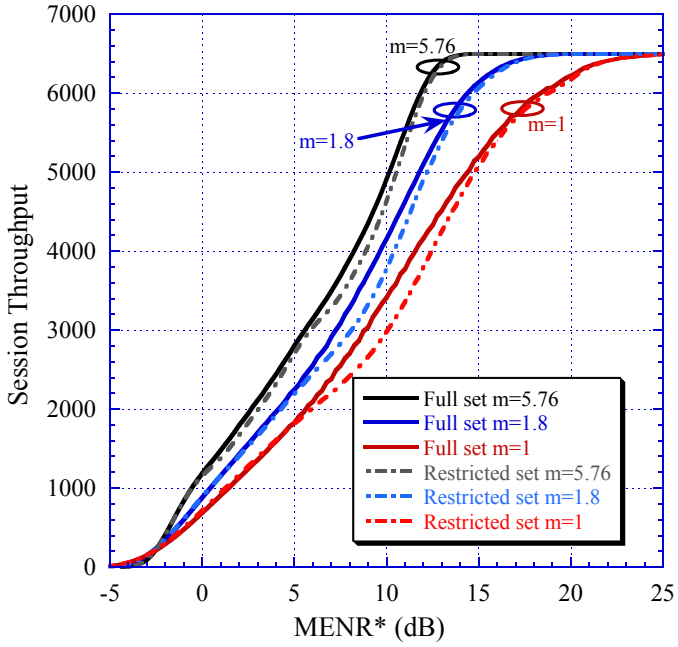

Figure 5.4: Throughput for PSI-P protocol with perfect channel state information with normalized Doppler $f_d T_s = 0.020$, comparing full set $\mathcal{A}$ to restricted set $\mathcal{A}'$, $\mathcal{N} = 64$ subcarriers, $\mathcal{G} = 4$ groups.

channel measurements or subchannel state information.

Different idealized perfect protocols and the AMCP are graphed in Fig. 5.5 for the Rayleigh fading channel for the relatively fast fading case and packets of length $L = 4096$. The hypothetical PSI-P protocol, which is given the previous state of the channel, outperforms the AMCP PO and AMCP SEC, but the difference between the PSI-P and AMCP PO averages only 1.0% when averages across the data points between MENR* of 0 and 20 dB. The AMCP SEC is only outperformed by the PSI-P protocol by 2.7% over that range. The AMCP SEC-WA falls about halfway between the AMCP PO and AMCP SEC, while the AMCP SEC-RT is closer to the AMCP SEC in performance. These two curves are not shown for legibility of the graph. Recall that the SEC ordering without using previous history to break ties or for a weighted average produces the least reliable ordering of everything considered, and the shorter packet size also decreases the accuracy of the

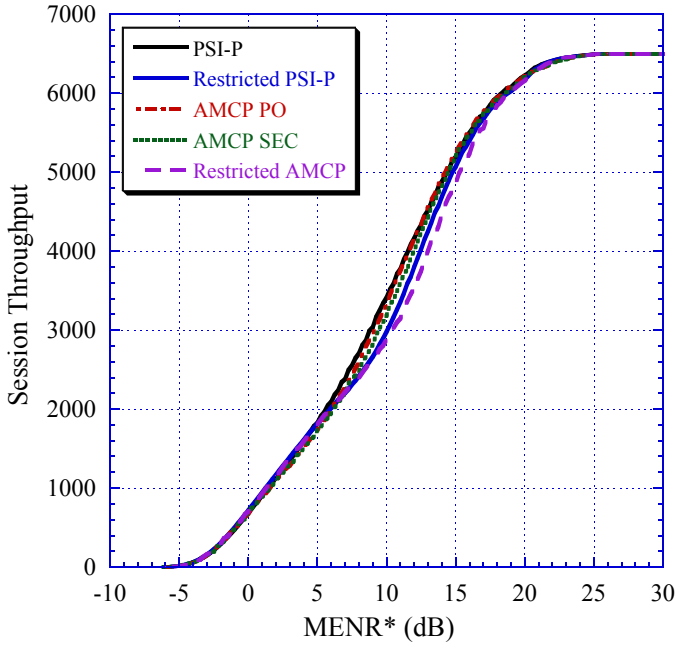

Figure 5.5: Throughput for adaptive and perfect protocols for fading channel with $m = 1$, $L = 4096$, $f_d T_s = 0.020$, $\mathcal{N} = 64$ subcarriers, $\mathcal{G} = 4$ groups.

subcarrier ordering. Despite these limitations the difference in performance between the AMCP SEC and AMCP PO, which uses the exact subcarrier ordering, is small. The graph also demonstrates the performance of the Restricted PSI-P and Restricted AMCP, which are limited to only using code-modulation assignments listed previously in Table 5.3. Even only using SEC ordering, the AMCP achieves higher session throughput than even the Restricted PSI-P, and the TER-based Restricted AMCP falls further behind.

Similar results can be seen for slower Rayleigh fading (lower normalized Doppler) in Fig. 5.6. The key difference when the fading is slower is that the PSI-P protocol performance improves relative to the AMCP. This is because the previous channel states give more information about future states, the PSI-P protocol can better exploit the fact that it chooses the modulation formats and code rate while knowing the resulting packet error rates for every such code-modulation assignment for those channel conditions. In other

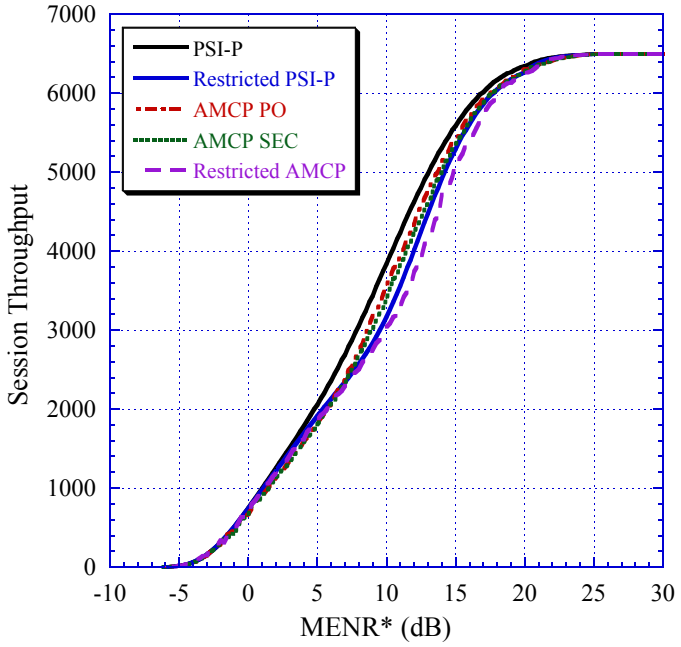

Figure 5.6: Throughput for adaptive and perfect protocols for fading channel with $m = 1$, $L = 4096$, $f_d T_s = 0.005$, $\mathcal{N} = 64$ subcarriers, $\mathcal{G} = 4$ groups.

words it has far more knowledge about the channel than would be reasonable, and it can fully exploit these advantages when the fading is slower. We still see that the AMCP SEC offers relatively good performance compared to the AMCP PO.

The session throughput for the AMCP again in the Rayleigh channel is shown in Fig. 5.7. Unlike in the other performance results, where it is assumed that there are $\mathcal{G} = 4$ groups of independently fading subcarriers, here it is assumed that all $\mathcal{N} = 64$ subcarriers are fading independently. In most fading channels, some correlation would be expected between some adjacent subcarriers, but because our proposed AMCP does not rely on any correlation structure between subcarriers for its operation, its performance is still good throughout the range of MENR*. Furthermore, a curve for the longer packet size of $L =$ 16384 symbols is shown; performance is almost the same as for the shorter size, with the most notable difference being between -3 and 0 dB. This is a result of requiring more

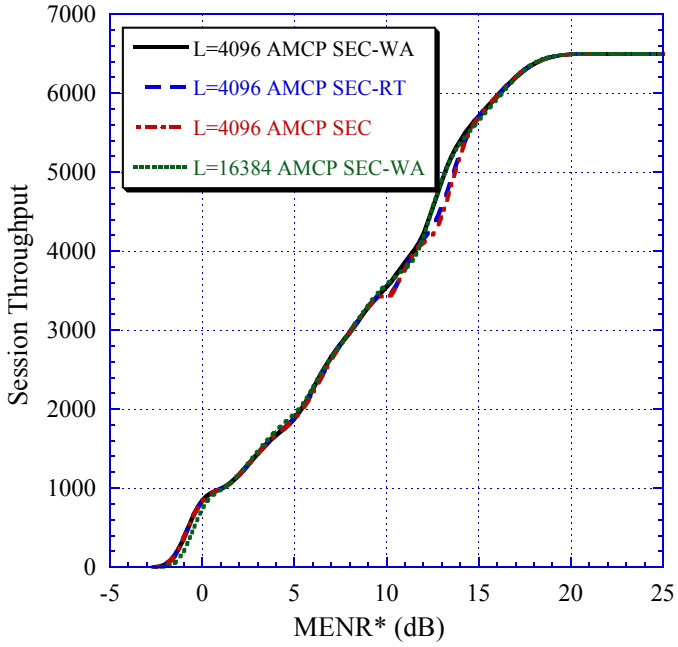

Figure 5.7: Throughput for adaptive protocols for fading channel with $m = 1$, $f_d T_s = 0.020$, $\mathcal{N} = 64$ subcarriers, $\mathcal{G} = 64$ groups.

code blocks per packet and thus having a higher probability of packet failure. Were a more powerful code used for the longer packet length, the performance would be expected to surpass that for $L = 4096$.

Between the range of 10 and 15 dB for MENR*, the AMCP SEC-WA outperforms the AMCP SEC-RT and AMCP SEC because here the latter two exhibit poorer subcarrier ordering, which leads to suboptimal modulation format assignments. At MENR$^* = 13$ dB, the average ordering error has a peak of 0.54 dB for the SEC and 0.40 dB for the SEC-RT for $L = 4096$. However, it is only 0.14 dB for the SEC-WA at $L = 4096$ and down to 0.07 dB for SEC-WA at $L = 16384$.

Though the focus so far has been on the Rayleigh fading channel, many communications systems operate under less severe fading, so those conditions are also of interest. The session throughput for the AMCP and PSI-P protocols, as well as the variants restricted

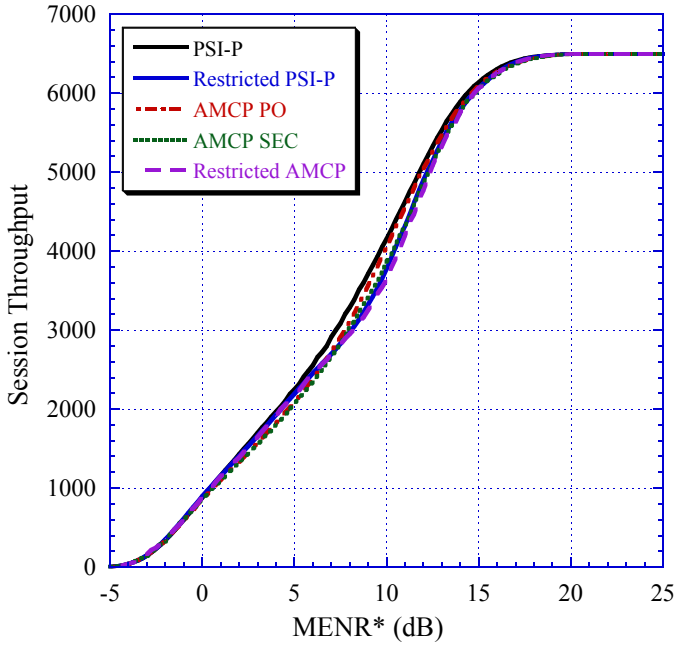

Figure 5.8: Throughput for adaptive and perfect protocols for fading channel with $m = 1.8$, $f_d T_s = 0.020$, $\mathcal{N} = 64$ subcarriers, $\mathcal{G} = 4$ groups.

to the smaller set, are shown in Figs. 5.8 and 5.9. For $m = 1.8$, the relative protocol performance is similar to $m = 1$, the Rayleigh fading case. However, with $m = 5.76$, which approximates Rician fading with a specular-to-diffuse ratio of 10, the conditions are much closer to a more AWGN-like channel. In this case, a relatively deep fade still keeps the subcarriers close together in terms of fade levels. The AMCP PO has comparable rather than superior performance compared to the the Restricted AMCP, with the AMCP SEC falling behind again (though again, the AMCP-WA falls between). This is because the adaptive modulation procedure in Section 5.3 does not produce rapid shifts between QPSK with a high code rate and 16-QAM with a lower code rate, which is what is necessary to perform better in such channels. Nevertheless, the AMCP is still shown to produce good performance in this relatively good channel. Its real advantage lies in being able to handle the faster and more severe fading channels.

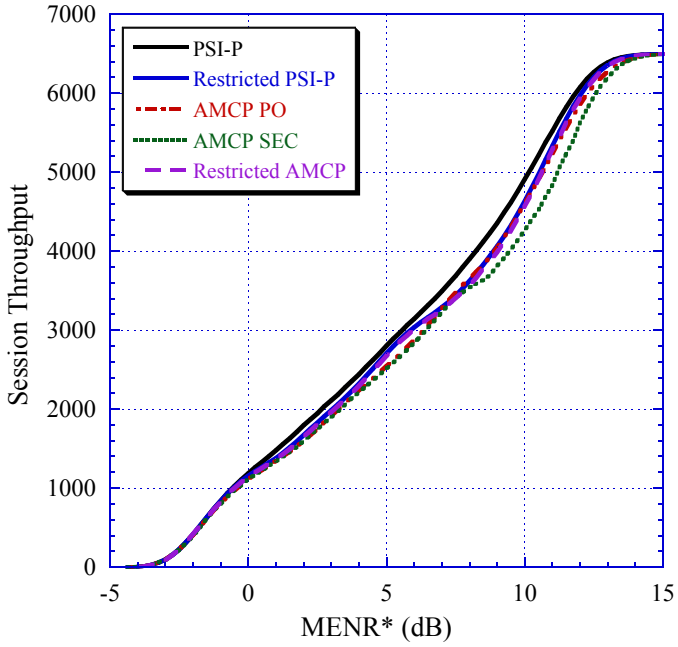

Figure 5.9: Throughput for adaptive and perfect protocols for fading channel with $m = 5.76$, $f_d T_s = 0.020$, $\mathcal{N} = 64$ subcarriers, $\mathcal{G} = 4$ groups.

Finally, a selected summary of some AMCP results is presented in Table 5.4. The session throughput and average ordering error can be seen for two different packet sizes and different subcarrier ordering algorithms. The results were not graphed because they are too close to be visually distinguishable. As expected, the SEC-WA ordering allows the AMCP to do the modulation format assignment more optimally, resulting in better performance than the SEC-RT and then the SEC. However, the parameter α for the ordering has some effect on the average ordering error, but it makes little difference on the final session throughput achieved. The plain AMCP SEC does respectably well, especially with the larger packet size, so in some systems the additional complexity of the SEC-RT and SEC-WA requiring memory of prior transmissions may not be worth the performance advantage. Furthermore, the session throughput for the AMCP detailed in Table 5.4 only considers fading; if there is an even more transient disturbance of the channel, it is possible

L	Ordering	α	Average Throughput	Ordering Error
4096	SEC	8	3397	0.3082
4096	SEC-RT	4	3402	0.2233
4096	SEC-RT	8	3403	0.2211
4096	SEC-RT	∞	3402	0.2232
4096	SEC-WA	4	3423	0.1546
4096	SEC-WA	8	3427	0.1408
4096	SEC-WA	∞	3425	0.1551
16384	SEC	8	3367	0.1454
16384	SEC-RT	4	3370	0.1101
16384	SEC-RT	8	3370	0.1060
16384	SEC-RT	∞	3370	0.1103
16384	SEC-WA	4	3366	0.0997
16384	SEC-WA	8	3375	0.0731
16384	SEC-WA	∞	3366	0.0999

Table 5.4: Average session throughput and average ordering error (dB), averaged across range of MENR* from 0 to 20 dB, $m = 1$, $f_d T_s = 0.020$, $\mathcal{G} = 4$ groups.

that performing weighted averages over old SECs may actually decrease performance.

Chapter 6

Conclusion

We have demonstrated how OFDM transmissions can be adapted from packet to packet to achieve good throughput in a variety of channel conditions. In particular, adaptive power loading, modulation, and coding were all considered for OFDM. However, power loading demonstrated little benefit for OFDM communications if robust forward error-control coding is used by the system. Adaptive modulation and coding without power loading can provide better performance and do not require as much information about the subchannel conditions, so we instead focused on developing an adaptive modulation and coding protocol (AMCP). Towards that end, we proposed novel methods for ordering subcarriers by estimated channel quality using subcarrier error counts. Unlike traditional techniques, this procedure relied only on information available from the decoder and does not require any channel measurements, which can be expensive to conduct accurately. In addition, these methods can accurately account for interference and other factors that channel measurement techniques may not detect.

The total error rate and the proposed subcarrier ordering techniques were sufficient for the AMCP to respond to changes in subchannel conditions. The total error rate can be computed from the subcarrier error counts, so all the statistics needed to operate the AMCP did not rely on any channel gain or signal-to-noise estimates, measurements, or prediction. Despite the simplicity of the metrics, the AMCP was able to achieve good performance

across a range of channel conditions. In some fading channels of interest, the AMCP achieved throughput similar to the perfect state information for the preceding packet (PSI-P) protocol, a hypothetical benchmark that always selects the code and modulation formats on each subcarrier that maximize the throughput for the subchannel states most recently experienced. Because of its suitability across different kinds of channels and the lack of assumptions and systems required regarding channel measurements, fading, interference, system nonlinearities, and so on, the AMCP should be practical means of improving the performance of many OFDM communications systems.

Bibliography

[1] J. Armstrong, "OFDM for optical communications," *Journal of Lightwave Technology*, vol. 27, no. 3, pp. 189–204, Feb. 2009.

[2] J.A.C. Bingham, "Multicarrier modulation for data transmission: an idea whose time has come," *IEEE Commun. Magazine*, May 1990.

[3] L.J. Cimini, Jr., "Analysis and simulation of a digital mobile channel using orthogonal frequency division multiplexing," *IEEE Trans. Commun.*, vol. 33, no. 7, pp. 665–675, Jul. 1985.

[4] L. Goldfeld, V. Lyandres, and D. Wulich, "Minimum BER power loading for OFDM in fading channel," *IEEE Trans. Commun.*, vol. 50, no. 11, pp. 1729-1733, Nov. 2002.

[5] J. Jiho and K. B. Lee, "Transmit power adaptation for multiuser OFDM systems," *IEEE J. Select. Areas Commun.*, vol. 21, no. 2, pp. 171-178, Feb. 2003.

[6] B. S. Krongold, K. Ramchandran, and D. L. Jones, "Computationally efficient optimal power allocation algorithms for multicarrier communication systems," *IEEE Trans. Commun.*, vol. 48, no. 1, pp. 23-27, Jan. 2000.

[7] D. Wang, Y. Cao, and L. Zheng, "Efficient two-stage discrete bit-loading algorithms for OFDM systems," *IEEE Trans. Veh. Technol.*, vol. 59, no. 7, pp. 3407-3416, Sep. 2010.

[8] Y. Li and W.E. Ryan, "Mutual-information based adaptive bit-loading algorithms for LDPC-coded OFDM," *IEEE Trans. on Wireless Commun.*, vol. 6, no. 5, pp. 1670–1680, May 2007.

[9] S. Nader-Esfahani and M. Afrasiabi, "Simple bit loading algorithm for OFDM-based systems," *IET Commun.*, vol. 1, no. 3, pp. 312–316, Jun. 2007.

[10] D. Dardari, "Ordered subcarrier selection algorithm for OFDM-based high-speed WLANs," *IEEE Trans. Wireless Commun.*, vol. 3, no. 5., pp. 1452–1458, Sep. 2004.

[11] S. Ye, R. S. Blum, and L. J. Cimini, Jr., "Adaptive OFDM systems with imperfect channel state information" *IEEE Trans. Wireless Commun.*, vol. 5, no. 11, pp. 3255–3265, Nov. 2006.

[12] M. R. Souryal and R. L. Pickholtz, "Adaptive modulation with imperfect channel information in OFDM," in *Proc. IEEE Intl. Conf. Commun. (ICC)*, vol. 6, pp. 1861–1865, Jun. 2001.

[13] Y. Rong, S. A. Vorobyov, and A. B. Gershman, "Adaptive OFDM techniques with one-bit-per-subcarrier channel-state feedback," *IEEE Trans. Commun.*, vol. 54, no. 11, pp. 1993–2003, Nov. 2006.

[14] E. H. Choi, W. Choi, J. G. Andrews, and B. F. Womack, "Power loading using order mapping in OFDM systems with limited feedback," *IEEE Signal Process. Lett.*, vol. 15, pp. 545–548, 2008.

[15] S. Nagaraj, "An extension to the ordered subcarrier selection algorithm (OSSA)," *IEEE Trans. Wireless Commun.*, vol. 8, no. 3, pp. 1159–1163, Mar. 2009.

[16] M. Nakagami, S. Wada, and S. Fujimura, "Some considerations on random phase problems from the standpoint of fading," *Inst. Electrical Commun. Engineers Proc.*, vol. 36, no. 11, pp. 595-602, Nov. 1953.

[17] M. Nakagami, "The m-distribution—A general formula of intensity distribution of rapid fading," in *Statistical Methods in Radio Wave Propagation*, W.C. Hoffman (ed.), pp.3-36, Pergamon Press, London, 1960.

[18] M. A. Juang and M. B. Pursley, "Finite-state Markov chain models for the intensity of Nakagami fading," *Int. J. Wireless Inform. Network.*, vol. 20, no. 2, 2013.

[19] G. Caire, G. Taricco, and E. Biglieri, "Bit-interleaved coded modulation," *IEEE Trans. Inf. Theory*, vol. 44, no. 3, pp. 926-946, May 1998.

[20] *Galaxy simulation tool kit user's guide*. Advanced Hardware Architectures (AHA). Product specification.

[21] J. G. Proakis, *Digital Communications*, 4th ed., McGraw-Hill, NY, 2001.

[22] A. Goldsmith, *Wireless Communications*, Cambridge U. Press, NY, 2005.

[23] H. S. Wang and N. Moayeri, "Finite-state Markov channel — A useful model for radio communication channels," *IEEE Trans. Veh. Technol.*, vol. 44, no. 1, pp. 163–171, Feb. 1995.

[24] M. A. Juang and M. B. Pursley, "Adaptation of modulation and coding for OFDM packet transmission," in *Proc. IEEE MILCOM*, pp. 1613-1618, Nov. 2010.

[25] M. Yu and P. Sadeghi, "A study of pilot-assisted OFDM channel estimation methods With improvements for DVB-T2," *IEEE Trans. Veh. Technol.*, vol. 61, no. 5, pp. 2400–2405, Jun 2012.

[26] J.-C. Chen, C.-K. Wen, and P. Ting, "An efficient pilot design scheme for sparse channel estimation in OFDM systems," *IEEE Commun. Lett.*, vol. 17, no. 7, pp. 1352–1355, July 2013.

[27] W. Li, Y. Zhang, L.-K. Huang, C. Maple, and J. Cosmas, "Implementation and co-simulation of hybrid pilot-aided channel estimation with decision feedback equalizer for OFDM systems," *IEEE Trans. Broadcast.*, vol. 58, no. 4, pp. 590–602, Dec. 2012.